Cosmology and cluster halo scaling relations

Araya-Melo, Pablo A.; van de Weygaert, Rien; Jones, Bernard J. T.

Published in:
Monthly Notices of the Royal Astronomical Society

DOI:
10.1111/j.1365-2966.2009.15565.x

Publication date:
2009

Monthly Notices
of the
ROYAL ASTRONOMICAL SOCIETY

Mon. Not. R. Astron. Soc. **400,** 1317–1336 (2009) doi:10.1111/j.1365-2966.2009.15565.x

Cosmology and cluster halo scaling relations

Pablo A. Araya-Melo,[1,2,3]★ Rien van de Weygaert[1] and Bernard J. T. Jones[1]

[1] *Kapteyn Astronomical Institute, University of Groningen, PO Box 800, 9700 AV Groningen, the Netherlands*
[2] *Korea Institute for Advanced Study, Dongdaemon-gu, Seoul 130-722, Korea*
[3] *Jacobs University Bremen, Campus Ring 1, 28759 Bremen, Germany*

Accepted 2009 August 17. Received 2009 August 10; in original form 2009 June 1

ABSTRACT

We explore the effects of dark matter and dark energy on the dynamical scaling properties of galaxy clusters. We investigate the cluster Faber–Jackson (FJ), Kormendy and Fundamental Plane (FP) relations between the mass, radius and velocity dispersion of cluster-sized haloes in cosmological *N*-body simulations. The simulations span a wide range of cosmological parameters, representing open, flat and closed Universes.

Independently of the cosmology, we find that the simulated clusters are close to a perfect virial state and do indeed define an FP. The fitted parameters of the FJ, Kormendy and FP relationships do not show any significant dependence on $\Omega_{\rm m}$ and/or Ω_Λ. One outstanding effect is the influence of $\Omega_{\rm m}$ on the thickness of the FP.

Following the time evolution of our models, we find slight changes of FJ and Kormendy parameters in high-$\Omega_{\rm m}$ universe, along with a slight decrease of FP fitting parameters. We also see an initial increase of the FP thickness followed by a convergence to a nearly constant value. The epoch of convergence is later for higher values of $\Omega_{\rm m}$, while the thickness remains constant in the low-$\Omega_{\rm m}$ Λ models. We also find a continuous increase of the FP thickness in the standard cold dark matter cosmology. There is no evidence that these differences are due to the different power spectrum slopes at cluster scales.

From the point of view of the FP, there is little difference between clusters that quietly accreted their mass and those that underwent massive mergers. The principal effect of strong mergers is to significantly change the ratio of the half-mass radius $r_{\rm half}$ to the harmonic mean radius $r_{\rm h}$.

Key words: galaxies: clusters: general – cosmological parameters – cosmology: theory – dark matter – large-scale structure of Universe.

1 INTRODUCTION

Recent observations of distant supernovae (Riess et al. 1998; Perlmutter et al. 1999) suggest that we are living in a flat, accelerated Universe with a low matter density. This accelerated expansion has established the possibility of a dark energy component which behaves like Einstein's cosmological constant Λ. A positive cosmological constant resolves the apparent conflict suggested by the old age of globular cluster stars, and the estimated value (Spergel et al. 2003, 2007) appears sufficient to yield a flat geometry of our Universe.

The role of Λ in the process of structure formation is not yet fully understood. Although its influence can be seen when looking at the global evolution of the Universe, its role in the dynamical evolution of cosmic structures is not clear. The most direct impact of Λ comes from its influence on the amplitude of the primordial perturbation power spectrum; there is also an influence from the change in the cosmic and dynamical time-scales. The direct dynamical influence is probably minor: we do know that in the linear regime it accounts for a mere $\sim$1/70th of the influence of matter perturbation (Lahav et al. 1991).

Most viable theories of cosmic structure formation involve hierarchical clustering. Small structures form first and they merge to give birth to bigger ones. The rate and history of this process are highly dependent on the amount of (dark) matter present in the Universe. In Universes with a low $\Omega_{\rm m}$, structure formation ceases at much early times than that in cosmologies with high-density values.

Within this hierarchical process, clusters of galaxies are the most massive and most recently formed structures in the Universe. Their collapse time is comparable to the age of the Universe. This makes them important probes for the study of cosmic structure formation and evolution. The hierarchical clustering history from which galaxy clusters emerge involves a highly complex process of

★E-mail: p.araya@jacobs-university.de

merging, accretion and virialization. In this paper, we investigate in how far we can get insight into this history on the basis of the internal properties of the clusters. This involves characteristics such as their mass and mass distribution, size, and kinetic and gravitational potential energy. In particular, we are keen to learn whether these do show any possible trace of a cosmological constant.

One particular profound manifestation of the virial state of cosmic objects is via scaling relations that connect various structural properties. Scaling relations of collapsed and virialized objects relate two or three fundamental characteristics. The first involves a quantity measuring the amount of mass M, often expressed in terms of the amount of light L emitted by the object. The second quantity involves the size of the object, while the third one quantifies its dynamical state. For a virialized halo with mass M, size R and velocity dispersion $\sigma_{\rm v} = \langle v^2 \rangle^{1/2}$, the implied scaling relation is

$$\log M \; = \; 2 \log \sigma_{\rm v} \; + \; \log R \; + \; \epsilon_M \, , \qquad (1)$$

where ϵ_M is a constant that reflects the internal dynamics of the system. (ϵ_M is determined by issues such as the isotropy of the cluster velocity dispersion, its shape and any substructure).

Systems having similar values of this constant would be expected to form a two-parameter family of objects: observationally, this manifests itself as the 'Fundamental Plane (FP)'. Objects lying on the same plane might be expected to have similar formation histories and, conversely, the nature of the FP is a clue to the underlying formation mechanism.

The scaling relations are of great importance for a variety of reasons. First of all, they inform us about the dynamical state of the objects and must be a profound reflection of the galaxy formation process (Robertson et al. 2006). Also, they have turned out to be of substantial practical importance. Because they relate an intrinsic distance-independent quantity like velocity dispersion to a distance-dependent one like $L_{\rm e}$, they can be used as cosmological distance indicators.

1.1 Observed relationships

1.1.1 Galaxies

Since the mid 70s, we know that the observed properties of elliptical galaxies follow scaling relations. The Faber–Jackson (FJ) relation (Faber & Jackson 1976) relates the luminosity L and the velocity dispersion σ of an elliptical galaxy. The Tully–Fisher relation (Tully & Fisher 1977) is the equivalent for spiral galaxies. A different, though related, scaling is that between the effective radius $r_{\rm e}$ and the luminosity L of the galaxy. This is known as the Kormendy relation (Kormendy 1977). These two relations turned out to be manifestations of a deeper scaling relation between three fundamental characteristics, which became known as the FP (Djorgovski & Davis 1987; Dressler et al. 1987).

The FP is generally expressed as a relationship between three parameters, though there is no consensus as to which three should best be used, nor precisely how to define them. This makes detailed comparisons somewhat difficult. Some authors use the set ($\log R$, $\log \sigma$, $\log I$), I being the luminosity in some spectral band within some radius R, while others use the set ($\log R$, $\log \sigma$, μ), μ being the mean surface brightness within that radius. Comparisons are further complicated by the fact that there appear to be manifest residual luminosity dependencies in the fits, as reported in a recent study of the Sloan Digital Sky Survey by Nigoche-Netro, Ruelas-Mayorgo & Franco-Balderas (2009).

Care is needed when interpreting these observed relationships. Observed data generally refer to luminosity rather than mass, and the radius that is used generally refers to some fiducial radius such as the half-light radius or some radius based on profile fitting. Often, the half-light radius, $R_{\rm e}$, as determined from a fit to a de Vaucouleurs profile is used.

This situation has been improved somewhat by the gravitational lensing study of Bolton et al. (2007). These authors presented a new formulation of the FP using lensing data to replace surface brightness with surface mass density. They also present an interesting alternative, which they refer to as the 'mass plane' (MP), in which they find the dependence of $\log(R_{\rm e})$ on $\log(\sigma_{\rm e2})$ and surface mass density $\Sigma_{\rm e2}$ within a radius $R_{\rm e}/2$. Using surface mass density $\Sigma_{\rm e2}$ within a radius $R_{\rm e}/2$ in place of surface brightness $I_{\rm e}$ removes one of the assumptions about the relationship between mass and light.

1.1.2 Galaxy clusters

Much recent galaxy cluster work on the FP has focused on the differences between the FPs of the clusters as defined by their member galaxies (see e.g. D'Onofrio et al. 2008 and references therein).

Galaxy cluster scaling relations were discovered by Schaeffer et al. (1993) who studied a sample of 16 galaxy clusters, concluding that these systems also populate an FP. Adami et al. (1998) used the ESO (European Southern Observatory) Nearby Abell Cluster Survey (ENACS) to study the existence of an FP for rich galaxy clusters, finding that it is significantly different from that for elliptical galaxies. Marmo et al. (2004) using data from the Wide-field Nearby Galaxy-cluster Survey (WINGS) cluster survey found that the difference is largely a simple shift in the relative positions of the planes.

The largely unknown relationship between mass and light frustrates a direct comparison with the results of N-body investigations.

1.2 Numerical investigations

Later, Lanzoni et al. (2004) addressed the question using N-body simulations for high-mass haloes, which are thought to host clusters of galaxies. On the basis of 13 simulated massive dark matter haloes in a ΛCDM cosmology, they found that the dark matter haloes follow the FJ-, Kormendy- and FP-like relations.

In hierarchical scenarios of structure formation, haloes build up by subsequent merging of smaller haloes into larger and larger haloes. Some of these mergers involve sizeable clumps, most involve a more quiescent accretion of matter and small clumps from the surroundings. This process leaves its mark on the phase-space structure of the haloes. Indeed, these dark halo streams are a major source of attention in present-day studies of the formation of our Galaxy (Helmi & White 1999; Helmi 2000).

It remains an interesting question as to whether we can find evidence for these merging events in the FP. González-García & van Albada (2003) look into the effects of major mergers on the FP and found that the FP does remain largely intact in the case of two merging ellipticals. However, what the effects will be of an incessant bombardment of a halo by material in its surroundings has not been studied in much detail. Given that this is a sensitive function of the cosmological scenario, we will study the influence on FP parameters and thickness in more detail.

In this paper, we address the specific question as to whether we can trace an influence of cosmic parameters in the scaling relations for simulated clusters, and in particular the influence of the cosmic density parameter $\Omega_{\rm m}$ and the cosmological constant Λ. We

use a set of dissipationless N-body simulations involving open, flat and closed Universes. All the simulations are variants of the cold dark matter (CDM) scenario, representing different cosmologies, concerning both different values for the mass density Ω_m, for dark energy Ω_Λ and for the implied power spectrum of density perturbations and the related merging and accretion history of the clusters.

The organization of this paper is as follows. In Section 2, we describe the simulations and the definitions of the various parameters we use. In Section 3, we present a general description of the scaling relations which we investigate in this study before specifying the way in which we analyse them from the cluster-sized haloes in our simulation. We investigate the scaling relations of galaxy clusters in different cosmologies at $z = 0$ in Section 4. Section 5 addresses the evolution of the scaling relations as a function of redshift and cosmic time. We also investigate the dependence of merging and accretion on the scaling relations, which we discuss in Section 6. The interpretation of our results on the FP within the context of the virial theorem is discussed in Section 7. Conclusions are presented in Section 8.

2 THE SIMULATIONS

We perform 13 N-body simulations that follow the dynamics of $N = 256^3$ particles in a periodic box of size $L = 200\,h^{-1}$ Mpc. The initial conditions are generated with identical phases for Fourier components of the Gaussian random field. In this way, each cosmological model contains the same morphological structures. For all models, we chose the same Hubble parameter, $h = 0.7$, and the same normalization of the power spectrum, $\sigma_8 = 0.8$. The principal differences between the simulations are the values of the matter density and vacuum energy density parameters, Ω_m and Ω_Λ. By combining these parameters, we get models describing the three possible geometries of the Universe: open, flat and closed. The effect of having the same Hubble parameter and different cosmological constants translates into having different cosmic times. Table 1 lists the values of the cosmological parameters and the cosmic times at which the data are analysed.

The initial conditions are evolved up to the present time ($z = 0$) using the massive parallel tree N-body code GADGET2 (Springel 2005). The Plummer-equivalent softening was set at $\epsilon_{pl} = 15\,h^{-1}$ kpc in physical units from $z = 2$ to 0, while it was taken to be fixed in comoving units at higher redshifts. For each cosmological model, we wrote the output of 100 snapshots, from $a_{exp} = 0.2$ ($z = 4$) to the present time, $a_{exp} = 1$ ($z = 0$), equally spaced in $\log(a)$.

2.1 Halo identification

We use the HOP algorithm (Eisenstein & Hut 1998) to extract the groups present in the simulations. HOP associates a density with every particle. In a first step, a group is defined as a collection of particles linked to a local density maximum. To make a distinction between a high-density region and its surroundings, HOP uses a regrouping procedure. This procedure identifies a group as an individual object on the basis of a specific density value. For this critical value, we chose the virial density value Δ_c based on the spherical collapse model. In order to have the proper Δ_c, we numerically compute its value for each of the cosmologies. See Table 1 for the values of the virial density for each cosmology at $z = 0$. For the latter, we list two values: the virial overdensity $\Delta_{vir,b}$ with respect to the background density ρ_b of the corresponding cosmology, and the related virial overdensity $\Delta_{vir,c}$ with respect to the critical density.

Note that we only consider groups containing more than 100 particles. Because the particle mass depends on the cosmological scenario, this implies a different mass cut for the haloes in each of our simulations. As a result, standard cold dark matter (SCDM) does not have groups with masses lower than $10^{13}\,h^{-1}\,M_\odot$. We have to keep in mind this artificial constraint when considering collapse and virialization in hierarchical scenarios at high redshifts, and also when making fits to the relationships among the various cluster parameters. In cases where structure growth is still continuing vigorously at the current epoch, the collapsed haloes at high redshifts will have been small: our simulations would not be able to resolve these.

2.2 Haloes and cosmology: an example

Fig. 1 follows the evolution of one particular cluster halo in four different cosmologies. These are ΛCDMO2 (open), ΛCDMF2 (flat), ΛCDMC2 (closed) and SCDM. By using the same Fourier phases to set up the initial conditions in each of the cosmologies, we get

Table 1. Cosmological parameters for the runs.

Model	Ω_m	Ω_Λ	Ω_k	Age	m_{dm}	m_{cut}	$\Delta_{vir,b}$	$\Delta_{vir,c}$
SCDM	1.0	0	0	9.31	13.23	1323	177.65	177.65
OCDM01	0.1	0	0.9	12.55	1.32	132	978.83	97.88
OCDM03	0.3	0	0.7	11.30	3.97	397	402.34	120.70
OCDM05	0.5	0	0.5	10.53	6.62	662	278.10	139.05
ΛCDMO1	0.1	0.5	0.4	14.65	1.32	132	838.30	83.83
ΛCDMO2	0.1	0.7	0.2	15.96	1.32	132	778.30	77.83
ΛCDMF1	0.1	0.9	0	17.85	1.32	132	715.12	71.51
ΛCDMO3	0.3	0.5	0.2	12.70	3.97	397	358.21	107.46
ΛCDMF2	0.3	0.7	0	13.47	3.97	397	339.78	101.93
ΛCDMC1	0.3	0.9	−0.2	14.44	3.97	397	320.79	96.237
ΛCDMF3	0.5	0.5	0	11.61	6.62	662	252.38	126.19
ΛCDMC2	0.5	0.7	-0.2	12.17	6.62	662	241.74	120.87
ΛCDMC3	0.5	0.9	-0.4	12.84	6.62	6622	30.85	115.43

Note. The first column gives the identification of the runs, and the following columns give the present matter density parameter, the density parameter associated with the cosmological constant, $\Omega_k = 1 - \Omega_m - \Omega_\Lambda$ quantifies the curvature of the Universe, the age of the Universe in Gyr since the big bang, the mass per particle in units of $10^{10}\,h^{-1}\,M_\odot$, the mass cut of the groups given by HOP in units of $10^{10}\,h^{-1}\,M_\odot$, the value of the (over)density needed to have virialized objects with respect to the background density, and similarly, but now with respect to the critical density.

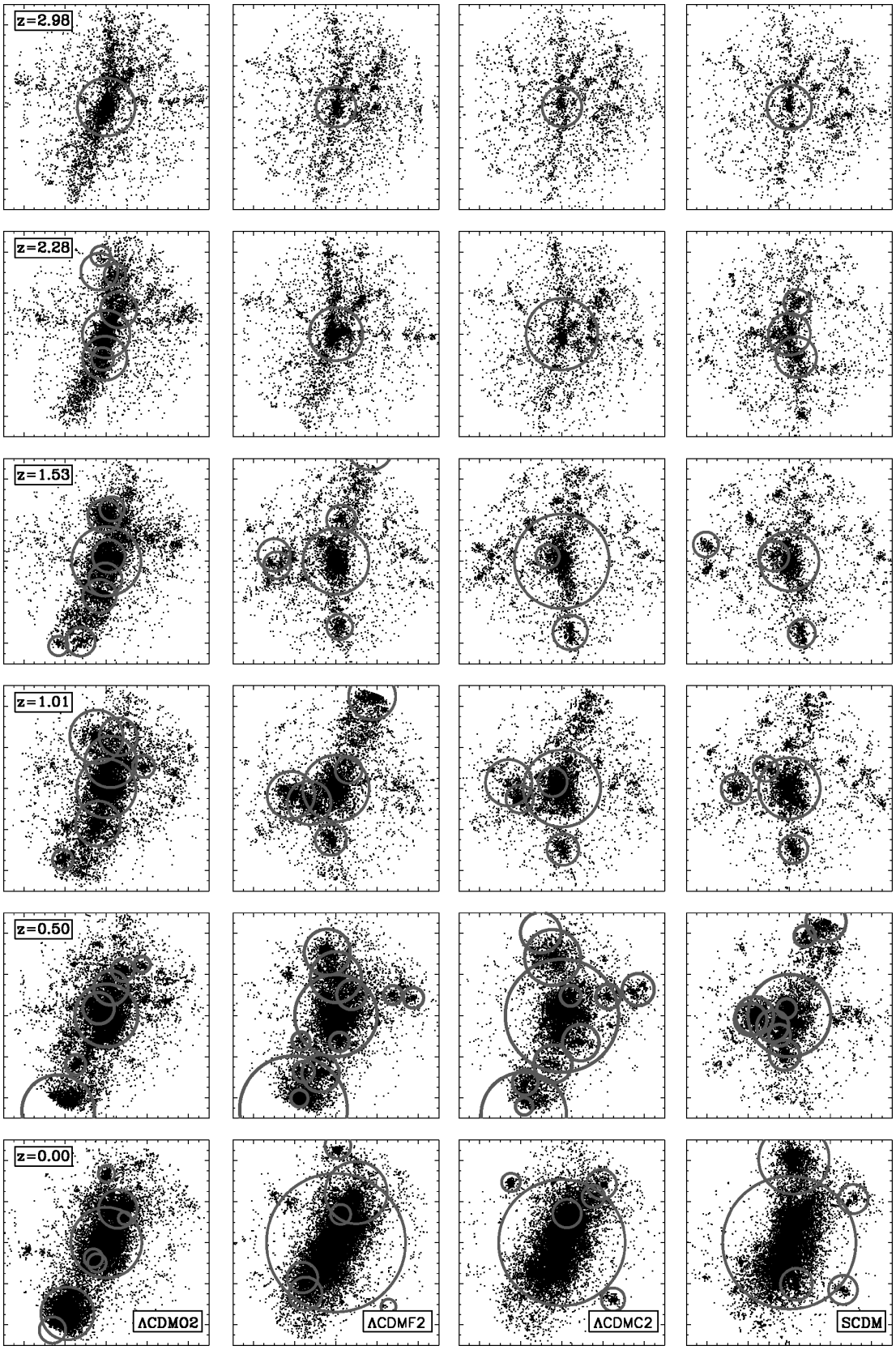

Figure 1. Cluster evolution: $\Omega_{\rm m}$ influence. Evolution as a function of redshift of a single dark matter halo in different cosmological models: ΛCDMO2, ΛCDMF2, ΛCDMC2 and SCDM. The dark matter particle distribution in a box of comoving size $5\,h^{-1}$ Mpc is shown at six different redshifts: $z = 2.98, 2.28, 1.53, 1.01, 0.50$ and 0.00. The circles correspond to haloes identified by HOP, with the size of the circle being proportional to their virial radius.

a sample of corresponding haloes. In each of the cosmologies, the evolution of the cluster halo is shown at six different redshifts, from $z \approx 3$ onwards to the present epoch $z = 0$. The panels show the mass distribution in and around the cluster, and its progenitors, in a box of comoving size $5\,h^{-1}$ Mpc. Circles enclose haloes identified by HOP, with the circle radius proportional to the virial radius of the group (i.e. the distance from the centre of mass to the outermost particle of the group). Projection effects may occasionally cause circles to appear within circles.

In all four cosmologies, the buildup of the halo clearly involves the merging of several smaller mass clumps, some of which are identified as genuine protohaloes by means of circles. Fig. 1 shows that the sequence ΛCDMO2, ΛCDMF2, ΛCDMC2 and SCDM corresponds to a sequence in which the formation of the halo shifts to later and later epochs. At all depicted redshifts, and in particular at higher redshifts, the clusters in the ΛCDMO2 cosmology have considerably more pronounced and developed mass concentration.

2.3 Halo properties

In our study, we limit ourselves to cluster-like haloes. A galaxy cluster is defined as a dark matter halo with a mass $M > 10^{14}\,h^{-1}\,\mathrm{M}_{\odot}$. We measure three quantities for each cluster and test their scaling relations.

Scaling relations of collapsed and virialized objects relate two or three fundamental characteristics of those objects. The first involves a quantity measuring the amount of mass, often in terms of the amount of light emitted by the object. The second quantity involves the size of the object, while the third one quantifies its dynamical state.

(i) *Mass:* defined as the number of particles multiplied by the mass per particle present in each group:

$$M = n_{\mathrm{part}} m_{\mathrm{part}}\,, \tag{2}$$

where n_{part} is the number of particles in the halo and m_{part} is the mass of each particle (see Column m_{dm} in Table 1). The mass of the particle is different for each cosmology.

(ii) *Surface mass density:* alternatively, following observational practice, we use the magnitude-scale surface mass density μ for our FP evaluations

$$\mu = -2.5 \log M + 5 \log r, \tag{3}$$

where M and r are the mass and the radius of the halo. Combining this with a mass-to-light ratio (M/L), it becomes a surface brightness, one of the observables of the FP.

(iii) *Velocity dispersion:* computed as

$$\sigma_{\mathrm{v}}^2 = \frac{2K}{n_{\mathrm{part}} m_{\mathrm{part}}}\,, \tag{4}$$

where K is the kinetic energy of the halo measured taking into account all the particles within the halo. Some perturbations are involved as a result of not removing interlopers, though we found that this did not systematically affect our results.

As a measure for the size of the haloes, we have explored two options: the half-mass radius and the mean harmonic radius.

(iv) *Half-mass radius:* r_{half} is the radius that encloses half of the mass of the clump. This radius is closest in definition to the half-light radius used in the observational studies.

(v) *Mean harmonic radius:* r_{h} is defined as the inverse of the mean distance between all pairs of particles in the halo:

$$\frac{1}{r_{\mathrm{h}}} = \frac{1}{N} \sum_{i<j} \frac{1}{|\boldsymbol{r}_{ij}|}\,, \qquad N = \frac{n_{\mathrm{part}}(n_{\mathrm{npart}} - 1)}{2}\,, \tag{5}$$

where $\boldsymbol{r}_{ij}$ is the separation vector between the ith and jth particles. The great virtue of this radius is that it is a good measure of the effective radius of the gravitational potential of the clump, certainly important when assessing the virial status of the clump. Also, it has the practical advantage of being independent of the definition of the cluster centre. To some extent, it is also an indicator of the internal structure of the halo because it put extra weight to close pairs of particles.

Most of the results presented in this paper refer to the mean harmonic radius of the haloes; this seems rather natural given that we are discussing the virial theorem. We have also compared the results obtained using the half-mass radii of the haloes.

In Fig. 2, we plot the mean harmonic radius versus the half-mass radius of the cluster-sized haloes in the SCDM and ΛCDMF2 models. We see that the relationship is not very tight at larger masses, and that the differences between the two radii are particularly prominent in the SCDM cosmology. We shall discuss this further in Section 6. Not surprisingly, the fitted FP parameters depend strongly on which radius is used. Equally surprising, the Kormendy relation slope does not seem to be particularly sensitive to the choice of r_{h} or r_{half} (the slopes are statistically not different). This is summarized in Table 6.

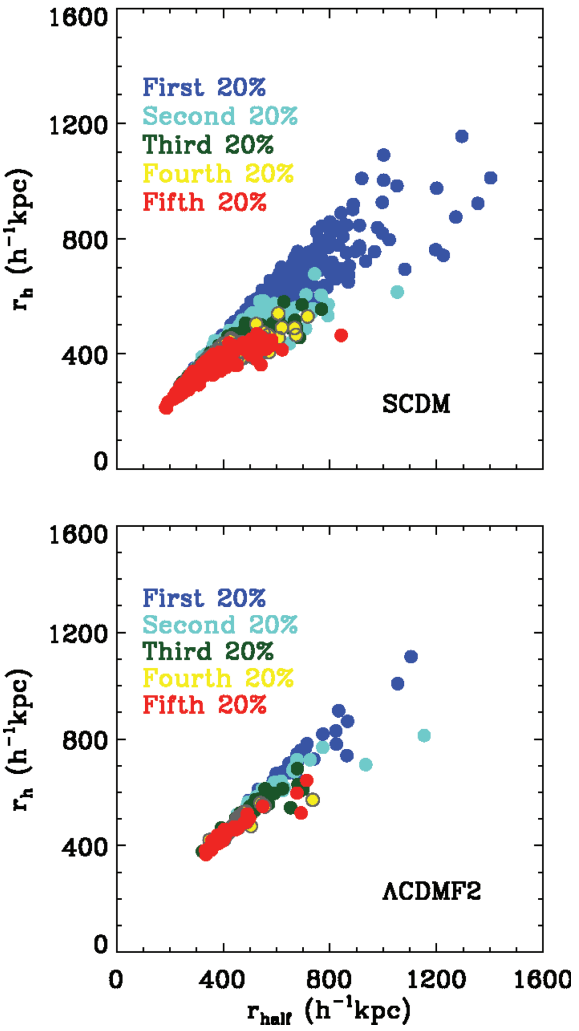

Figure 2. Comparison between the mean harmonic and the half-mass radii of the cluster-sized haloes in the SCDM (top panel) and ΛCDMF2 (bottom panel) scenarios. The colours depict different mass ranges, each colour representing a 20 percentile mass quantile.

3 SCALING RELATIONS

For the samples of cluster-sized haloes in our simulations, we will be assessing three specific scaling relations: the FJ relation, the Kormendy relation and the FP.

From observations of elliptical galaxies, we have learned that there are tight scaling relations between a few of their fundamental structural properties (see e.g. Binney & Merrifield 1998). These properties are the total luminosity L of a galaxy – or its surface brightness μ – its characteristic size R_e and its velocity dispersion σ_v.

3.1 Faber–Jackson and Kormendy relations

The first scaling relation is the FJ relation (Faber & Jackson 1976) between the luminosity L of the galaxy and its velocity dispersion σ_v,

$$L \propto \sigma_v^{\beta}\,, \tag{6}$$

where the index $\beta \sim 4$. A similar relation, known as the Tully–Fisher relation (Tully & Fisher 1977), holds for H I discs of spiral galaxies. According to this relation, the galaxies' rotation velocity is tightly correlated with the absolute magnitude of the galaxy.

Another relation was established by Kormendy (1977). He found that there is a strong, not entirely unexpected, correlation between the luminosity L and effective radius R_e of the elliptical galaxies:

$$L \propto R_e^{\alpha}\,, \tag{7}$$

where the index $\alpha \sim 1.5$.

3.2 Galaxy Fundamental Plane

Both the FJ and Kormendy relations relate two structural characteristics and should be seen as projections of a more fundamental and tight relation between all three structural quantities: the FP. The FP of elliptical galaxies was first formulated by Djorgovski & Davis (1987) and Dressler et al. (1987). When we take the three-dimensional space defined by the effective radius R_e of the galaxy, its surface brightness I_e (with total luminosity $L \propto I_e R_e^2$) and velocity dispersion σ_v, we find that they do not fill space homogeneously but instead define a thin plane.

In logarithmic quantities, this plane may be parametrized as

$$\log R_e = \gamma \log I_e + \delta \log \sigma_v + C_{FP}. \tag{8}$$

For example, Jørgensen, Franx & Kjaergaard (1996) found that a reasonable fit to the FP is given by

$$\log R_e = -0.82 \log I_e + 1.24 \log \sigma_v + C_{FP}. \tag{9}$$

While nearly all galaxies, ranging from giant ellipticals to compact dwarf ellipticals, appear to lie on the FP (also see e.g. Jørgensen, Franx & Kjaergaard 1995; Bernardi et al. 2003; Cappellari et al. 2006; Bolton et al. 2007), it is interesting to note that diffuse dwarf ellipticals do not (Kormendy 1987); they seem to be fundamentally different objects.

The observed FP not only provides information on the dynamical state of the object but also on the evolution of its stellar content and, by implication, about its formation. For a virialized object with effective radius R_e and M/L, the FP relation will have the form

$$\log R_e = -\log I_e + 2 \log \sigma_v - \log (M/L) + C_s\,, \tag{10}$$

in which $I_e = L/4\pi R_e^2$ is the mean surface brightness and C_s is a constant dependent on the structure of the object.

The observed parameter values for elliptical galaxy FP (see equation 9) are different from what might be expected for a plane that results simply from virialization and constant M/L. One explanation for this difference is that galaxies may be structurally equivalent while having a mass-dependent M/L. That would imply a formation process involving a tight fine-tuning of M/L. Nevertheless, pursuing this view, the parameters inferred by Jørgensen et al. (1996) (equation 9) would imply a M/L dependence on mass:

$$(M/L) \propto M^{0.25}\,, \tag{11}$$

using $M \propto \sigma_v^2 R_e$ and $L \propto I_e R_e^2$ (see e.g. Faber 1987). Recent semi-analytical modelling of galaxy formation suggests a more complex relation between the M/L and luminosity, involving a minimum M/L for galaxies with $M \approx 10^{11}$–$10^{12}\,h^{-1}\,\mathrm{M}_\odot$. In the absence of any M/L dependency, the discrepancy between the planes would have to be due to variations in the structure parameters of the galaxies.

There is an intrinsic scatter of the FP that has been found for elliptical galaxies; this has not been completely explained and may be a manifestation of the formation process.

A slightly different approach is used in the gravitational lensing study of Bolton et al. (2007). These authors presented a new formulation of the FP using lensing data to replace surface brightness with surface mass density, arriving at the relationship of the form

$$\log R_e = \gamma \log I_e + \delta \log \sigma_{e2} + C_{FP}\,, \tag{12}$$

where σ_{e2} is the velocity dispersion within half of the effective radius R_e, and

$$\gamma = -0.78 \pm 0.13, \quad \delta = 1.50 \pm 0.32, \quad C_{FP} = 3.9 \pm 1.7. \tag{13}$$

Furthermore, they suggest that the scatter about the FP, derived from their data, correlates with their derived M/L for the galaxies in their sample. The evidence is not strong though it is suggestive.

They also present an interesting alternative, which they refer to as the MP, in which they find the dependence of $\log(R_e)$ on $\log(\sigma_{e2})$ and surface mass density Σ_{e2} within a radius $R_e/2$:

$$\log R_e = \gamma_m \log \Sigma_{e2} + \delta_m \log \sigma_{e2} + C_{FP,m} \tag{14}$$

with

$$\gamma_m = -1.16 \pm 0.09,\ \delta_m = 1.77 \pm 0.14,\ C_{FP} = 7.8 \pm 1.0. \tag{15}$$

Using surface mass density Σ_{e2} within a radius $R_e/2$ in place of surface brightness I_e removes one of the assumptions about the relationship between mass and light.

3.3 Cluster Fundamental Plane

If clusters were fully virialized objects with the same internal dynamics, they would necessarily lie on a universal FP in the mass–velocity–radius space. This was first addressed by Schaeffer et al. (1993), who, using sample of 29 Abell clusters, discovered an FP relation in light–velocity–radius space: $L \propto R_e^{0.89} \sigma_v^{1.28}$. This is equivalent to the relationship

$$\log R_e = -0.90 \log I_e + 1.15 \log \sigma_v + C_{FP}, \tag{16}$$

in which I_e is a measure of the mean surface brightness of the cluster. The corresponding FJ relation is $L \propto R_e^{1.87}$ and the Kormendy relation is $L \propto R_e^{1.34}$. Similar numbers were inferred by Lanzoni et al. (2004), $L \propto R_e^{0.90} \sigma_v^{1.31}$.

In a project designed to test this further, Adami et al. (1998) found an FP relation for a sample of ENACS clusters, though their fitted

parameters were markedly different: $L \propto R^{1.19\pm0.14}\,\sigma^{0.91\pm0.16}$. This is equivalent to the relationship

$$\log R_{\rm e} = -(1.23 \pm 0.20)\log I_{\rm e} + (1.12 \pm 0.11)\log\sigma_{\rm v} + C_{\rm FP}\,, \tag{17}$$

in which $I_{\rm e}$ is the mean surface brightness of the cluster. Note that there are considerable systematic uncertainties in these values which are not reflected in the quoted error bars: these arise out of the profile fitting to the cluster. The above fit to the data is based on fitting a King profile (this gave the best fit to the data).

In studies of simulated dark matter dominated galaxy clusters, we can study scaling relations that are similar to those inferred from observable quantities. To infer these relations, we base ourselves on the mass M of the object. If the selected objects have the same average density, we would expect an equivalent Kormendy relation given by

$$M \propto R_{\rm e}^3\,. \tag{18}$$

Any difference in slope should be ascribed to a dependence of mean density $\langle\rho(R_{\rm e})\rangle$ on the size $R_{\rm e}$ of the object. The equivalent FP relation will be that of equation (1), while the FJ relation would then be

$$M \propto \sigma_{\rm v}^3\,. \tag{19}$$

Note that this is based on the assumption of constant mean density ρ of the selected objects, in line with HOP overdensity criterion (see Section 2.1).

Lanzoni et al. (2004) analysed the N-body cluster scaling relations on the basis of a sample of 13 massive dark matter haloes identified in a high-resolution ΛCDM N-body simulations. They were able to confirm the existence of FP relations for the simulation dark matter clusters and also found that these have a slope that was significantly different from the galaxy FP slope,

$$\log R_{\rm e} = (0.44 \pm 0.02)\,\mu + (1.92 \pm 0.12)\log\sigma_{\rm v} + C_{\rm FP}\,, \tag{20}$$

with μ being the surface mass density (equation 3). The difference in FP parameters between the dark matter haloes and those inferred for the observed cluster sample (see equation 16) formed a key aspect of their study. They suggest that a mass-dependent cluster M/L

$$(M/L) \propto M^{0.8} \tag{21}$$

would be able to explain the observed cluster FP. Interestingly, this is markedly different from that inferred for early-type galaxies. Of course there is no obvious reason why the FP for galaxies should have any bearing on the FP for clusters. Indeed, as we shall see for the ENACS sample, its FP parameter values seem to be irreconcilable with the virial theorem.

3.4 Determination of scaling relations

For the sample of N cluster-sized haloes in each simulation, we study the scaling relations between their size r, mass M – or equivalent surface mass density μ – and velocity dispersion σ (note that N is in general different for each cosmology). Given the inferred mass M (equation 2), velocity dispersion $\sigma_{\rm v}$ (equation 4) and the mean harmonic radius $r_{\rm h}$ (equation 5) of the cluster haloes, we find the scaling relation parameters by linear fitting of the relations.

Sample selection effects play a complex role in the analysis of real data samples (La Barbera et al. 2003). Fortunately, the issue is far simpler when analysing clusters found in N-body models where the only selection criterion is a mass cut-off imposed by the cluster finding algorithm. We deal with that simply by making the mass of the cluster the independent variable in all fits where relevant: this eliminates biases introduced through this object selection.

3.4.1 *Kormendy relation*

For the Kormendy relation, we fit

$$\log r = a\,\log M + C_a \tag{22}$$

to the N data points $(\log r_i, \log M_i)$ of the halo sample. As a measure for the significance of the fit, we use the standard deviation $\mathcal{S}_{\rm K}$,

$$\mathcal{S}_{\rm K} = \sqrt{\frac{1}{(N-1)}\sum_i^N (\log r_i - a\log M_i - C_a)^2}. \tag{23}$$

3.4.2 *Faber–Jackson relation*

Along the same line, the FJ relation is determined on the basis of the fit

$$\log\sigma_{\rm v} = b\,\log M + C_{\rm b}\,. \tag{24}$$

As a measure for the significance of the fit, we use the standard deviation $\mathcal{S}_{\rm FJ}$,

$$\mathcal{S}_{\rm FJ} = \sqrt{\frac{1}{(N-1)}\sum_i^N (\log\sigma_{{\rm v},i} - b\log M_i - C_{\rm b})^2}. \tag{25}$$

3.4.3 *Fundamental Plane*

Instead of fitting the FP in the form of equation (1), we do it in the way suggested by the observational work, i.e. using the surface mass density μ and velocity dispersion $\sigma_{\rm v}$ as free parameters from which we determine a model for the radius,

$$\log r = c\mu + d\,\log\sigma_{\rm v} + C_{\rm FP}\,. \tag{26}$$

In this, μ is the magnitude-scale surface mass density (equation 3). Although there are errors in determining both $\sigma_{\rm v}$ and μ, they are very small when compared with the dispersion about the FP. By fitting the parameters c and d this way we solve problems regarding biases in the mass (luminosity) selection.

As a measure for the significance of the FP fit, we use the standard deviation of the N simulation cluster haloes perpendicular to the plane,

$$\mathcal{S}_{\rm FP} = \sqrt{\frac{1}{(N-2)}\sum_i^N (\log r_i - c\mu_i - \log\sigma_{\rm v} - C_{\rm FP})^2}\,. \tag{27}$$

The thickness $w_{\rm FP}$ of the FP is estimated on the basis of the perpendicular distances of the cluster haloes to the fitted plane:

$$w_{\rm FP} = \sqrt{\frac{\sum D_\perp^2}{N}}\,, \tag{28}$$

where N is the number of cluster haloes in the sample and $D_\perp$ is the perpendicular distance of a point to a plane

$$D_\perp = \frac{c\mu + d\log\sigma_{\rm v} + C_{\rm FP} - \log r_{\rm h}}{(c^2+d^2+1)^{1/2}}\,. \tag{29}$$

4 SCALING RELATIONS IN DIFFERENT COSMOLOGIES: $z = 0$

We first investigate the scaling relations of the cluster dark matter haloes in our cosmological models at the current epoch, $z = 0$, and look for possible systematic differences between the parameter values and FP thickness as a function of the cosmology. The parameters of the resulting linear fits, to be discussed in the following sections, are listed in Table 3.

4.1 Kormendy relation

Fig. 3 shows the relation between the mean harmonic radius r_h of each cluster halo and their mass M (see Section 2.3). Each of the four panels depicts the relation for the haloes in one particular simulated cosmology. The top-left panel shows the SCDM cosmology, the top-right one the ΛCDMO2 model, the bottom-left one the ΛCDMF2 model and the bottom-right one the ΛCDMC2 model.

In each cosmology, there is a strong and systematic almost linear relation between $\log M$ and $\log r_h$: the Kormendy relation appears to be a good description for all situations. A visual comparison between SCDM relation (top-left panel), the ΛCDMO2 relation (top-right panel) and the ΛCDMF2 relation (bottom-left panel) shows that clusters of comparable mass have a larger size in the low-Ω_m cosmology than in the ones with a higher density value. In other words, clusters are more compact in the SCDM cosmology. Not unexpectedly we find objects of a higher density in higher Ω_m models.

When fitting the plotted point distributions, we infer the parameter values listed in Table 3. In each of the panels in Fig. 3, we plotted the linear fits for all of the four depicted cosmologies. We find similar slopes for all cosmologies, of the order of $a \sim 0.36$–0.38. This seems to imply that the mean density $\langle \rho(r_h) \rangle \propto M^{-0.1}$: more massive haloes have a slightly lower average density (see also Lanzoni et al. 2004). To investigate the dependence of the Kormendy parameter a on the cosmology in Fig. 4, we have plotted the slope a as a function of the average mass density parameter Ω_m (top panel), as a function of the cosmological constant Ω_Λ (central panel) and as a function of the cosmic curvature, in terms of $\Omega_{total} = \Omega_m + \Omega_\Lambda$ (lower panel). There is no evidence for any systematic trends of the Kormendy parameter as a function of cosmology. No evidence for an influence of either cosmic density Ω_m and Ω_Λ on the internal structure of the haloes could be detected.

4.2 Faber–Jackson relation

Fig. 6 shows the Faber–Jackson relation: the relation between the mass M and the velocity dispersion σ_v of the cluster haloes (see Section 2.3). Like in Fig. 3, each of the four panels corresponds to one particular simulated cosmology: SCDM (top-left panel), ΛCDMO2 (top-right panel), ΛCDMF2 (bottom-left panel) and ΛCDMC2 (bottom-right panel).

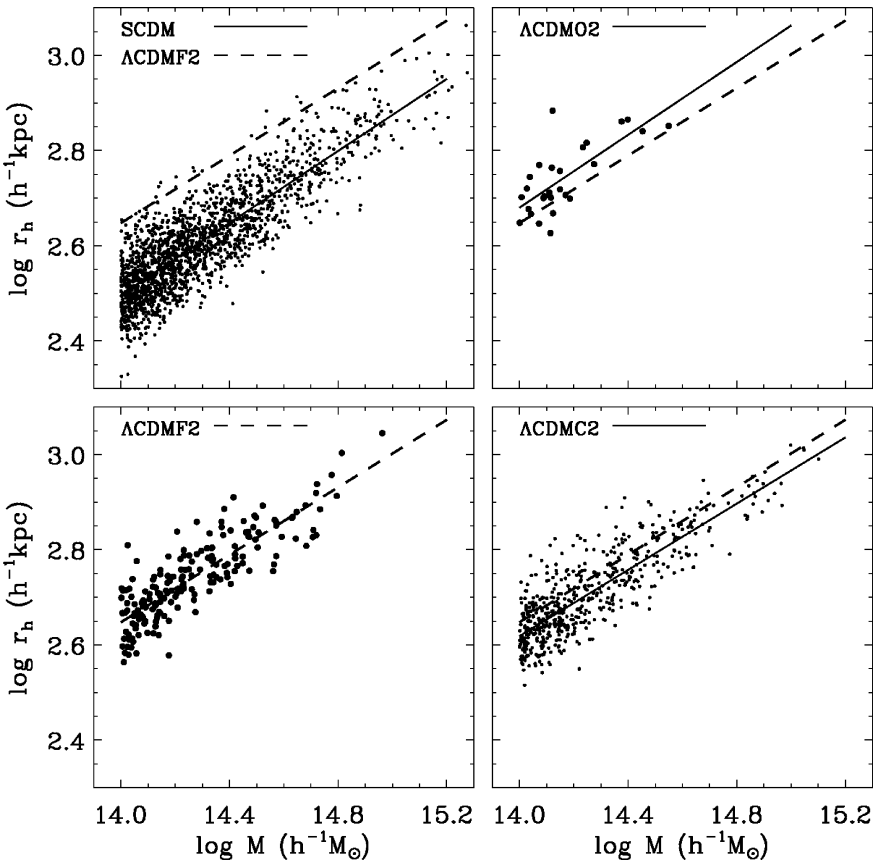

Figure 3. The Kormendy relation. Each panel plots the relation between mean harmonic radius r_h and mass M of the cluster-sized dark haloes in the simulations corresponding to one particular cosmology. Going from top-left to bottom-right panels, these are SCDM, ΛCDMO2, ΛCDMF2 and ΛCDMC2. In each of the panels, we have superimposed the fitted Kormendy relation for the corresponding model and for ΛCDMF2 as comparison.

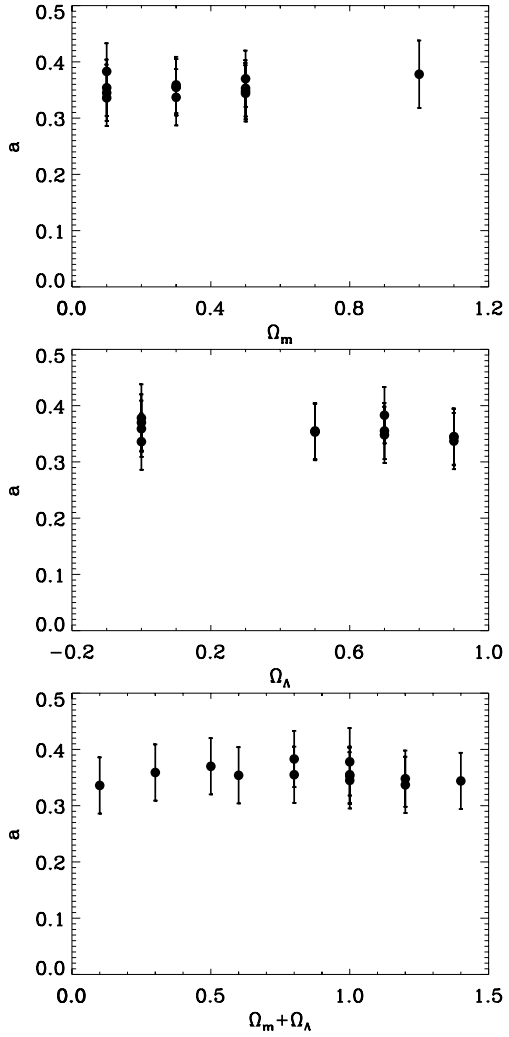

Figure 4. Inferred parameter a for the Kormendy relation (equation 22) as a function of Ω_m (top panel), Ω_Λ (central panel) and $\Omega_m + \Omega_\Lambda$ (bottom panel). The bars represent the 1σ uncertainty range around the estimated parameter.

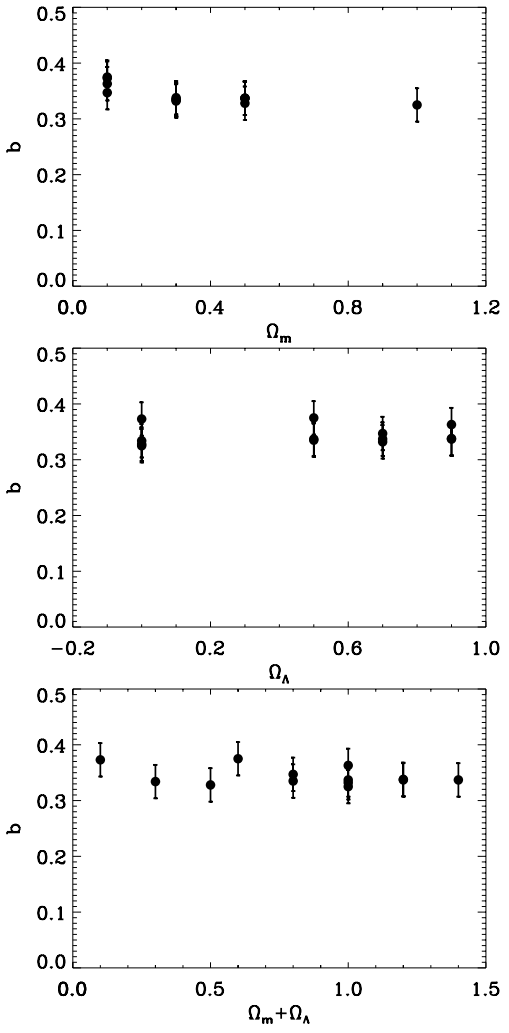

Figure 5. Inferred scaling parameter b for the FJ relation as a function of three different parameters: Ω_m (top panel), Ω_Λ (central panel) and $\Omega_m + \Omega_\Lambda$ (bottom panel). The bars represent the 1σ uncertainty range around the estimated parameter.

For comparison, in each of the panels we show the line of the ΛCDMF2 model corresponding to the linear fit of this relation in each of the depicted cosmologies. The M–σ_v relation is clearly well fitted by the Faber–Jackson like relation. It is considerably tighter than the equivalent Kormendy relation.

It is also interesting to note that, as with the Kormendy relation, we do not find any significant dependence of the FJ relation on the underlying cosmology: the slope b in all cases is of the order of $b \sim 0.35$ (see Table 3). We also did not find any dependence on Ω_Λ or Ω_{total} (see Fig. 5).

Although the difference between the inferred value of $b \sim 0.35$ in most cosmologies and the value of $b = 0.33$ expected for virialized perfectly homologous systems (see equation 19) is not really significant, the consistent and systematic value $b > 0.33$ might be suggestive for a weakly homologous population along the lines described in , for example, Bertin, Ciotti & Del Principe (2002).

4.3 Fundamental Plane

The Kormendy relation and the Faber–Jackson relation are two-dimensional projections of an intrinsically three-dimensional relation between mass M, size r and velocity dispersion σ_v of the haloes (see Section 2.3). Each of the four panels. By implication, the spread of the FP relation should be less than that of each of the previous two relations.

The FP obtained for the same cosmologies as shown in Figs 3 and 6 (SCDM, ΛCDMO2, ΛCDMF2 and ΛCDMC2) is illustrated in Fig. 7. In each of the frames, we have plotted the harmonic radius r_h of the haloes against the quantity $Y = c\mu + d \log \sigma_v + C_{FP}$ on a log–log plot (see Section 4.4 and Fig. 8 for scaling relations for alternative radius definition). The parameters c and d in the latter quantity, Y, combining the surface mass density μ and the velocity dispersion σ_v of each halo are the best-fitting FP parameters for the corresponding cosmology (see Table 3).

The galaxy clusters in each cosmology do indeed seem to populate a tightly defined plane. The point clouds in each of the frames confirm our expectation that they should have a much lower scatter around the plane than in the case of the Kormendy and Faber–Jackson relation (see Table 2).

From Table 3, we find a surprising level of consistency between the FPs in each of the cosmologies. We find that the inferred parameters are close to the one theoretically expected for perfectly

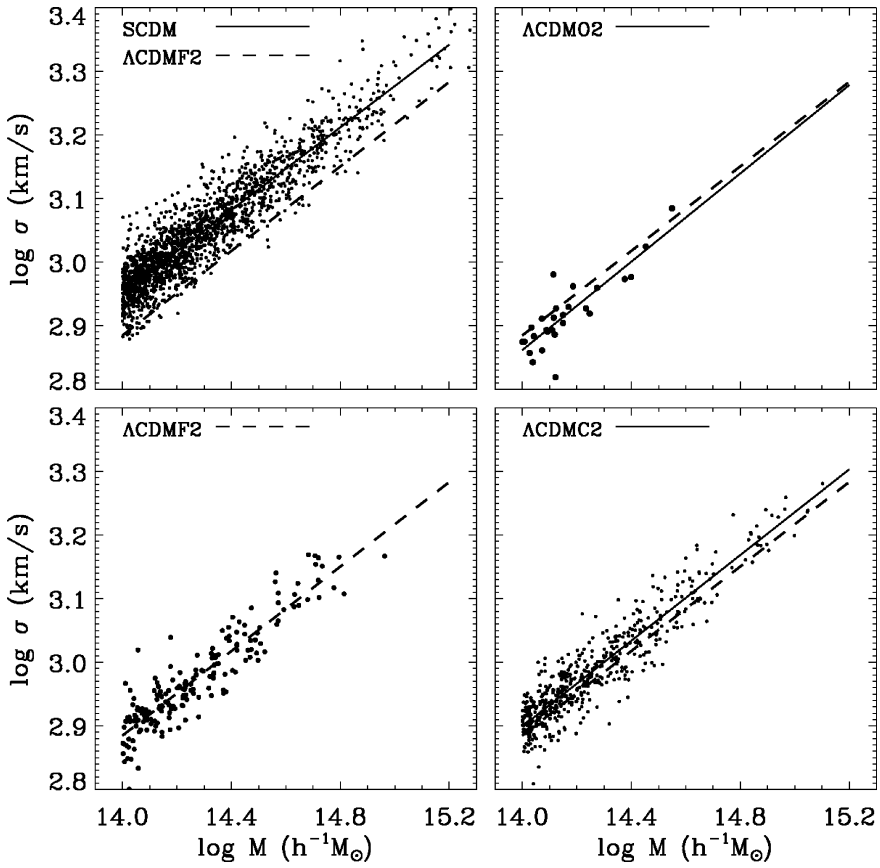

Figure 6. The FJ relation. Each panel plots the relation between the velocity dispersion σ_v and the mass M of the cluster-sized dark haloes in the simulations corresponding to one particular cosmology. Going from top-left to bottom-right panels, these are SCDM, ΛCDMO2, ΛCDMF2 and ΛCDMC2. In each of the panels, we have superimposed the fitted FJ relation for the corresponding model and for ΛCDMF2 for comparison.

homologous virialized clusters haloes. The inferred scaling parameter c for the surface density μ hovers around 0.38–0.42, close to the theoretical value $c \approx 0.4$ ($M \propto r_h \sigma_v^2$). The difference is somewhat larger for the parameter d, implying that the velocity dispersion scaling has a difference of ∼0.15–0.25 from the theoretical value of 2.

As can be seen in both Table 2 and Fig. 7, there is hardly any variation between the FP relations in the different cosmologies: they almost all coincide. This is certainly true concerning the FP parameters c and d. The top two panels of Fig. 9 do confirm the impression that there is no systematic difference as a function of Ω_m and/or Ω_Λ. This in itself is a strong argument against differences in the scaling relation parameters being due to a partial or incomplete level of virialization, as was claimed by Adami et al. (1998).

One possible difference between the FP in different cosmologies may concern its thickness w_{FP}. Inspection of Fig. 7 does suggest a marginally lower thickness of the FP for Universes with a low $\Omega_m \sim 0.1$. There is no detectable effect at all with respect to the cosmological constant Ω_Λ. We might understand a dependence on Ω_m, or cosmological constant Ω_Λ, in terms of the ongoing evolution of the cluster population. In low-Ω_m Universes – and in high-Ω_Λ universes – all clusters formed at high redshift and have since had ample time to reach full virialization and hence tighten the corresponding FP. In high-Ω_m Universes, clusters would still undergo a substantial levels of merging and accretion, both of which may affect the virial state of the cluster. Our computer experiments do not seem to find any strong and significant dependence on overall cosmology.

We investigate the relationship between the FP thickness and the dynamical state of the cluster in more detail in Section 6.

Finally, we can try to relate the FP (μ, r_h, σ_v) of our simulated cluster samples to the observationally measured (L, R_e, σ_v) plane, for example $L \propto R^{1.19}\,\sigma^{0.91}$ found for the ENACS survey. We can ask whether the difference can be ascribed solely to a mass-dependent M/L.

4.4 Scaling relations for alternative radius definition

Apart from the mean harmonic radius that we have used as a measure of halo size in the previous sections, we have also assessed the viability of the scaling relations in case of alternative size definitions. In Table 4, we list the resulting parameters for the Kormendy relation and the FP in the case of using the half-mass radius r_{half}.

The parameters for the Kormendy relation hardly differ from the ones inferred on the basis of the mean harmonic radius. However, the inferred FP parameters do differ significantly from the ones inferred above on the basis of the mean harmonic radius. The change in scaling parameter values may be ascribed to the use of quantities that probe different aspects of the structure and dynamics of the haloes. In an extreme situation, this might have disrupted the scaling relations. Our finding shows that the Kormendy relation still holds, while the FP relation still holds but in a slightly different guise. It may be an indication for our contention that haloes do not form a perfectly homologous population. Size measures sensitive to different aspects of the haloes' internal mass distribution may then result in somewhat different scaling properties. In this respect, we

Table 2. Parameters of the scaling relations derived for the galaxy clusters in each of the simulated cosmological simulations.

Model	Ω_m	Ω_Λ	$r_h \propto M^a$		$\sigma \propto M^b$		$\log r_h = c\mu + d\log\sigma + C_{FP}$					
			a	$\mathcal{S}_K$	b	$\mathcal{S}_{FJ}$	c	σ_c (10^{-2})	d	σ_d (10^{-2})	$\mathcal{S}$	w_{FP} (10^{-3})
SCDM	1	0	0.38	0.06	0.33	0.03	0.37	0.31	1.78	1.14	0.03	14.03
OCDM01	0.1	0	0.34	0.05	0.37	0.03	0.35	1.73	1.60	8.27	0.02	8.57
OCDM03	0.3	0	0.36	0.05	0.33	0.03	0.38	1.10	1.76	4.13	0.03	13.41
OCDM05	0.5	0	0.37	0.05	0.33	0.03	0.37	0.53	1.79	2.01	0.03	12.24
ΛCDMO1	0.1	0.5	0.35	0.05	0.38	0.03	0.37	1.55	1.60	7.56	0.02	7.51
ΛCDMO2	0.1	0.7	0.38	0.05	0.35	0.03	0.38	1.90	1.66	8.84	0.02	8.44
ΛCDMF1	0.1	0.9	0.35	0.05	0.36	0.03	0.38	1.64	1.69	7.93	0.01	6.97
ΛCDMO3	0.3	0.5	0.36	0.05	0.34	0.03	0.41	1.03	1.86	3.88	0.03	11.43
ΛCDMF2	0.3	0.7	0.36	0.05	0.33	0.03	0.41	1.11	1.88	4.01	0.02	11.23
ΛCDMC1	0.3	0.9	0.34	0.05	0.34	0.03	0.42	1.19	1.92	4.33	0.03	11.09
ΛCDMF3	0.5	0.5	0.35	0.05	0.34	0.03	0.38	0.56	1.81	2.10	0.03	11.75
ΛCDMC2	0.5	0.7	0.35	0.05	0.34	0.03	0.38	0.57	1.82	2.14	0.03	11.66
ΛCDMC3	0.5	0.9	0.34	0.05	0.34	0.03	0.39	0.61	1.83	2.31	0.03	12.24

Note. r_h is the mean harmonic radius of the cluster. a is the scaling parameter for the Kormendy relation, b is the scaling parameter for the FJ relation and c and d are the scaling parameters for the FP. σ is the standard error in each of the scaling relation parameters, $\mathcal{S}$ is the corresponding standard error/significance of the fit.

agree with the conclusions of Adami et al. (1998) and Lanzoni et al. (2004).

See Sections 6 and 7 for a discussion of the relationship between the radii r_{half} and r_h, where we show that it is a consequence of the cluster building process.

5 EVOLUTION OF SCALING RELATIONS

In the previous sections, we have extensively studied the scaling relations at the current cosmic epoch $z = 0$. We have also noted that there are differences between the scaling relation parameters that we find in our simulations and those for perfect virialized and homologous systems. This makes it interesting to trace the evolution of the different scaling relations.

In this section, we investigate the evolution of the scaling relations as a function of redshift and as a function of cosmic look-back time. While observers usually think in terms of redshift, it is important to appreciate that a given redshift corresponds to an entirely different dynamical epoch in different cosmologies. Given the same Hubble parameter, the age of the Universe is a sensitive function of the cosmic density parameter Ω_m and even more so of the cosmological constant. As for the latter, we have to realize that the change in cosmic time as a function of the cosmological constant is the most important influence of Λ. To give an appreciation of the differences in cosmic time for a given redshift in the different cosmologies, we refer to Table 3.

We have probed the scaling relations over a range of redshifts from $z = 4$ to 0 and over a range of cosmic look-back time going from 1 to 10 Gyr. The evolution of the fitted scaling parameters as a function of redshift is shown in the left-hand column of Fig. 10. The corresponding evolution as a function of cosmic look-back time can be found in the right-hand column. The Kormendy parameter a is shown in the top panels, the Faber–Jackson parameter b in the centre panels and the FP parameters c and d in the bottom panels. Each different cosmology is represented by a different line style, listed in the insert at the top-left frame.

Table 3. Cosmic times in Gyr and the corresponding redshift for a set of four reference cosmological models.

Cosmic time	SCDM	ΛCDMO2	ΛCDMF2	ΛCDMC2
2.36	1.49	4	2.71	2.21
3.26	1.01	2.92	1.98	1.60
4.06	0.74	2.35	1.56	1.24
5.07	0.50	1.83	1.19	0.93
9.31	0	0.71	0.38	0.24

5.1 Evolution of the Kormendy relation

For all cosmologies, the evolution of the Kormendy relation is marginal at best. In the case of the low-Ω_m ΛCDMO2 cosmology, we cannot discern any significant change of the parameter a (this may in part be due to the large uncertainties in the calculated parameter resulting from the low number of haloes in this simulation). In the case of the other cosmologies, we find no notable change of a before a redshift $z \approx 2$, followed by a mild increase from $a \approx 0.3$ to 0.38 at $z \approx 0$. This is also clearly visible when assessing the evolution in terms of cosmic time, as can be seen in the top-right panel.

5.2 Evolution of the Faber–Jackson relation

Evolutionary trends for the FJ relation are comparable to that seen in the Kormendy relation. No discernible trends are found in the open cosmology, while all of the other high-density Universes do show a mild decrease from $b \approx 0.35$ at $z \approx 2$ to $b \approx 0.32$ at $z \approx 0$. When assessing in terms of cosmic time (centre-right panel), we observe a near uniform increase of b over the last 8 Gyr.

In most studied cosmologies, with the possible exception of the ΛCDMO2 cosmology, we find a marginal trend of the FP parameter c to decrease for $z < 2$, more or less in the past ∼6–7 Gyr. At earlier epochs, such a trend is entirely absent. No significant evolution of the FP parameter d can be observed in Fig. 10.

5.3 Evolution of the Fundamental Plane

No significant evolution has been found for the FP parameters c and d (see Fig. 10, lower panels). Evolution of the FP mainly concerns its thickness.

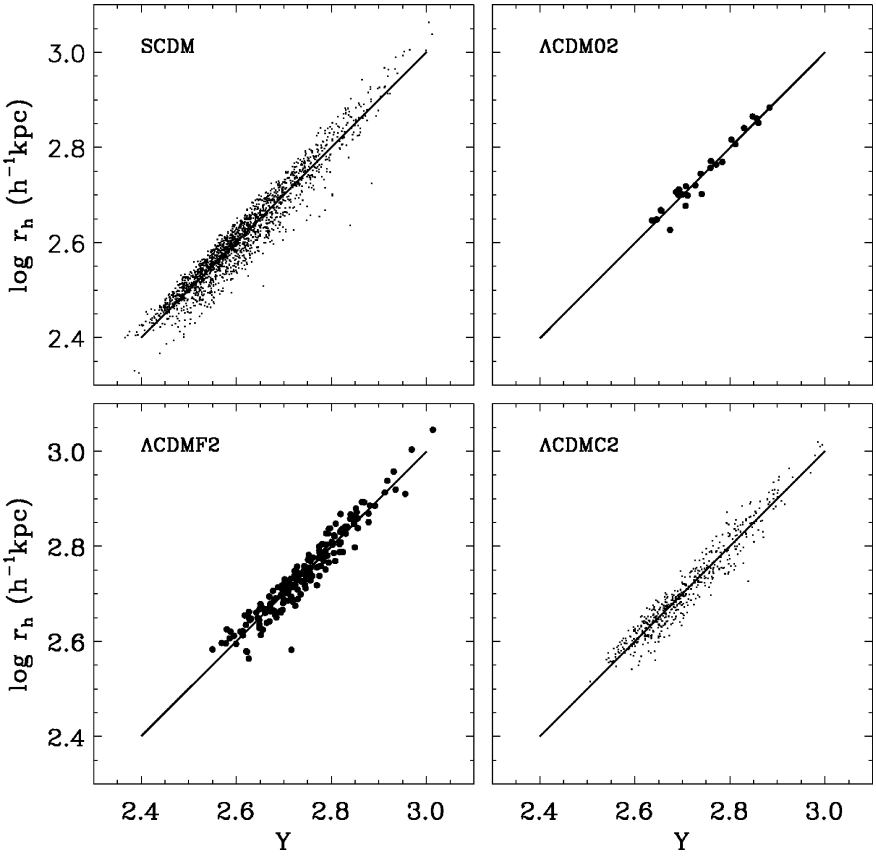

Figure 7. The FP. Each panel plots the relation between harmonic radius $r_{\rm h}$ and the quantity $Y = c\mu + d \log\sigma$. Combining the surface mass density μ and velocity dispersion $\sigma_{\rm v}$, the scaling parameters c and d are the ones inferred from the FP fitting procedure. Top-left panel: the relation between harmonic halo radius $r_{\rm h}$ and Y for the cluster halo sample in the SCDM simulation. Top-right panel: for the haloes in the ΛCDMO2 simulation. Bottom-left panel: for the haloes in the ΛCDMF2 simulation. Bottom-right panel: for the haloes in the ΛCDMC2. The superimposed lines in each panel represent the relation for the fitted FP for the corresponding cosmology. Note that, by definition, each of these fitted lines should have slope unity.

In Fig. 11, we show the development of the FP thickness as a function of cosmic expansion factor $a_{\rm exp}(t) = 1/(1+z)$ for four cosmological models, and in Figs 12 and 13 we show the evolution of the spread of points with the FP as a function of redshift in the ΛCDMF2 model.

We see a systematic increase of the FP thickness over the whole cosmic evolution in the case of the high-$\Omega_{\rm m}$ SCDM cosmology. While we do see a rise of the FP thickness before $a_{\rm exp} < 0.5$ in the ΛCDMF2 and ΛCDMC2 cosmologies, after that time the increase levels off and may even flatten completely. Note, however, that these simulations do not attain sufficient halo mass resolution at higher redshifts: in these cosmologies, haloes still are low-mass objects at these epochs. One exceptional cosmology is that of the low-$\Omega_{\rm m}$ Universe ΛCDMO2. Except for a rather abrupt and sudden jump in the FP thickness at $a_{\rm exp} \sim 0.3$, there is no notable change at later epochs. By $a_{\rm exp} = 0.3$, nearly all its clusters are in place and define an FP that does not undergo any further evolution.

In summary, the trend seems to be for initial increase of the FP thickness followed by a convergence to a nearly constant value. The epoch of convergence is later for higher values of $\Omega_{\rm m}$; while the thickness remains constant for the low-$\Omega_{\rm m}$ ΛCDMO2 cosmology, it involves a slow but continuous increase in the SCDM cosmology.

On the basis of their study of galaxy merging, Nipoti, Londrillo & Ciotti (2003) argued that the disposition of galaxies in the FP is not simply a realization of the virial theorem, but contains additional information on galaxy structure and dynamics. This should be reflected in the location of the halo population within the FP.

Figs 12 and 13 show how the location of the clusters within the plane shifts as time proceeds. The colour scheme is the same as for Fig. 2. Fig. 12 shows the location of the clusters in the ΛCDMF2 cosmology in the FP inferred for the current epoch, i.e. at redshift $z = 0$,

$$\log r_{\rm h} \,=\, 0.41\,\mu \,+\, 1.88\,\log\sigma_{\rm v} \,+\, C_{\rm FP,L}\,. \qquad (30)$$

To locate their position within the FP, we use the (artificial) coordinates F_1 and F_2 of the halo points with respect to two mutually perpendicular normalized vectors in the FP at $z = 0$, with respect to the coordinate system defined by the FP quantities $(\log r_{\rm h}, \mu, \log\sigma_{\rm v})$ (note that F_1 and F_2 do not have a specific physical significance). From the panels in the figure, we see that the evolution of haloes involves a gradual shift along an almost universal FP. It also shows that the halo population seems to evolve from a more scattered and somewhat looser one into a tightly elongated point cloud at the current epoch, providing interesting clues towards understanding the cluster virialization process.

In the same vein, Fig. 13 follows the changing location of clusters in the SCDM cosmology in the corresponding FP at $z = 0$,

$$\log r_{\rm h} \,=\, 0.37\,\mu \,+\, 1.78\,\log\sigma_{\rm v} \,+\, C_{\rm FP,S}\,. \qquad (31)$$

Similar to the ΛCDMF2 cosmology, we find that the cluster point cloud appears to assume a clearer mass stratification as time proceeds. While the population of clusters in the SCDM cosmology

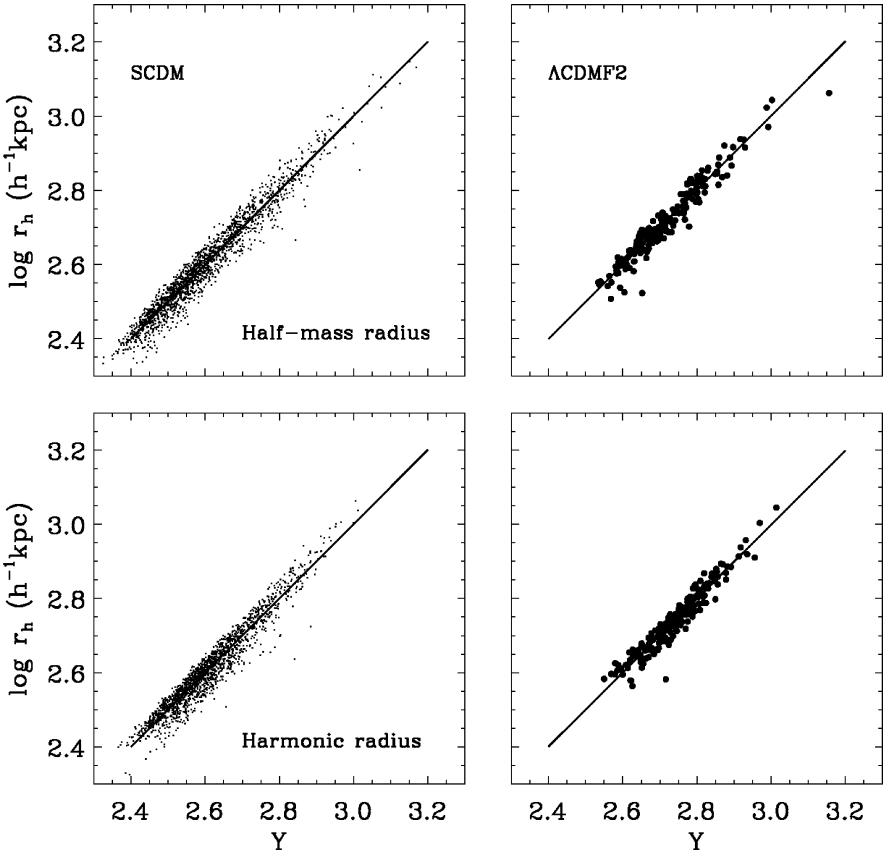

Figure 8. The FP relation of dark haloes in the SCDM (left-hand panels) and ΛCDMO2 (right-hand panels) cosmology, using the half-mass radius $r_{\rm half}$ (top row) and the harmonic radius $r_{\rm h}$ (bottom row). Plotted are mass M versus the FP quantity $Y = c\mu + d\log\sigma$, with c and d being the scaling parameters inferred from the (linear) fitting procedure. The lines represent the best-fitting FP relations.

also appears to shift its location along the FP as it evolves, we do not find a trend towards a more tightly point cloud that we see in the LCDMF2 cosmology. We will investigate these evolutionary trends in more detail in an upcoming study, we have found indications for a possible influence of the different cluster halo merging histories in SCDM and ΛCDMF2 in explaining the different behaviours of the cluster point clouds in the FP.

6 MERGING AND ACCRETION DEPENDENCE

Figs 10 and 11 show that the evolution of the parameters defining these relationships is very erratic. This testifies to the fact that in hierarchical structure formation scenarios the formation and evolution of haloes are hardly quiescent and steadily progressing affairs. Rather, haloes grow in mass by steady accretion of matter from its surrounding as well through the merging with massive peers. Even the accretion is not a continuous and spherically symmetric process: most matter flows in a strongly anisotropic fashion through filamentary extensions into the neighbouring large-scale matter distribution. As a result, we can expect that many haloes will not have settled into a perfect virial state. This will certainly be the case for haloes that recently suffered a major merger with one or more neighbouring clumps.

The detailed accretion and merging history is a function of the underlying cosmology. Low-density cosmologies or cosmologies with a high cosmological constant will have frozen their structure formation at early epochs. The haloes that had formed by the time of that transition will have had ample time to settle into a perfect virialized object. Also, there is a dependence on the power spectrum of the corresponding structure formation scenario. Power spectra with a slope $n < -1.5$ (at cluster scales) will imply a more homologous collapse of the cluster-sized clumps, less marked by an incessant bombardment by smaller clumps. It may be clear that a more violent life history of a halo will usually be reflected in a substantial deviation from a perfect virial state.

In order to investigate the implications of a difference in accretion or merging history of haloes, we have split the samples of cluster haloes in each of our cosmologies into a *merging sample* and an *accretion sample*. Possible differences in their virial state should be reflected in the quality of the scaling relations, in particular that of the thickness of the FP.

The *merger sample* consists of those haloes that suffered a merger with another halo that contained at least 30 per cent of its mass. Fig. 14 shows two examples of haloes in the ΛCDMF2 cosmology. The top sequence of four panels shows the evolution of a quiescently evolving *accretion halo*, by means of the particle distribution in a $5\,h^{-1}$ Mpc box (comoving size) around the cluster core, at $z =$ 2.61, 1.61, 0.89 and 0.00. The circles indicate the location of the HOP identified haloes, with the size of the circle proportional to the radius of the halo (note that the overlap of circles is due to the projection of the halo spheres). The lower group of four panels shows the particle distribution at the same redshifts for a halo belonging to the *merging sample*. Its gradual hierarchical buildup is directly visible as the continuous infall of clumps at each time-step.

In Fig. 15, we show the evolution of the thickness of the FP for each of the two samples in the four indicated cosmologies. Note

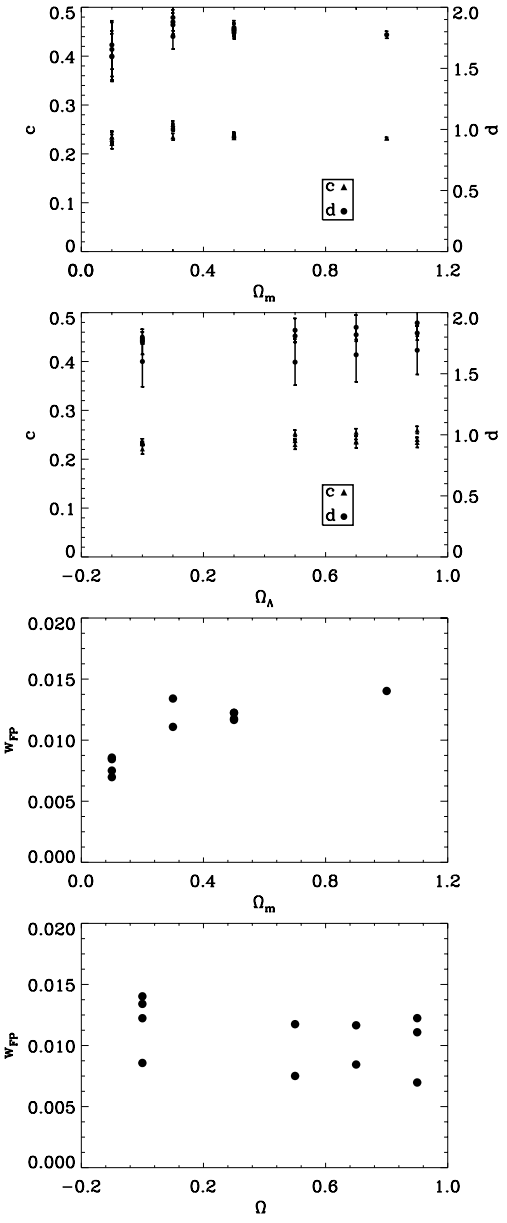

Figure 9. Top panel: FP parameters c (left-hand axis, solid circles) and d (right-hand axis, solid triangles) as a function of Ω_m. Second panel: FP parameters c (left-hand axis, solid circles) and d (right-hand axis, solid triangles) as a function of Ω_Λ. Third panel: thickness w_{FP} of the FP, i.e. rms scatter of the FP relation as a function of Ω_m. Bottom panel: thickness w_{FP} of the FP, i.e. rms scatter of the FP relation as a function of Ω_Λ.

that our simulations do not have sufficient resolution for reconstructing the precise merging or accretion history before $a_{exp} = 0.3$–0.4, so that we may not draw conclusions on the rise of the FP thickness up to that epoch. Also, in the case of the ΛCDMO2 scenario we do not have enough cluster haloes to be able to detect any systematic differences between the merging and accreting haloes.

In the more recent history, we do find some significant differences between merging and accretion-only haloes in various cosmologies, in particular the ones with a high Ω_m. There does not seem to be a systematic difference between these groups in the ΛCDMF2 cosmology. The total absence of any difference between the FP of merging and accreting cluster haloes at present (Fig. 16) is the outcome of an evolutionary history without any significant differences between the two subsamples (Fig. 15, lower-left panel).

The story is quite different for the ΛCDMC2 and SCDM cosmologies. While the cluster haloes that undergo a major merger do reveal a constantly growing FP thickness, their accretion-only clusters do not display such a systematic increase. Instead, their FP thickness remains lower and levels off. In other words, accretion haloes (dotted lines) do on average display a tighter FP relation. This is particularly true at the current epoch. Apparently, the absence of violent mass gain in the case of accretion haloes implies that they have more time to relax and virialize. This, in turn, is reflected in a thickness of the FP which does not evolve any further. Interestingly, it is also reflected in the radii of the haloes (Fig. 17): while the harmonic and half-mass radii of accreting cluster haloes are mostly in accordance with each other, though with a larger spread than in the case of ΛCDMF2 clusters (lower panel), the SCDM haloes that underwent major mergers do appear to be responsible for the substantial differences between the harmonic and half-mass radii that we see in Fig. 2. From this we conclude that the accretion history is a major factor in determining the character of the FP, via the impact of mergers on the mass distribution within haloes and hence their radii. We discuss this in more detail in Section 7.

The implications of this finding might be far reaching. Given the remarkable robustness and stability of the FP, any deviation of individual clusters from the FP may be a direct reflection of its recent dynamical evolution. This would be true if the thickness of the plane would be entirely due to the merger history of the clusters. It is certainly a viable implication of our conclusion that the FP's definition – the average plane of a large sample of clusters – is nearly unassailable while we find strong fluctuations and deviations from the average FP in small samples of actively evolving clusters.

In practice, it might mean that one could take samples of clusters in different redshift bands and reliably average them in each band to use the resulting FP to study redshift evolution of observed samples. It would also mean that within each redshift band you know which ones have had active lives.

7 RECONCILING THE SIMULATIONS WITH THE VIRIAL THEOREM

7.1 The virial theorem

The FP is a direct reflection of the virial theorem which, under particular assumptions, relates the averaged velocity dispersion and radius of a system directly to its mass. All 'virialized' objects will lie on a plane defined in the space of those three variables. There is not even any freedom in the parameters for that plane: its slope and location are fixed for all virialized objects.

There are complications when assigning data to an FP. First, in its simplest form, the virial theorem assumes that the virialized objects are isolated spherical systems and, importantly, that they are stationary. The systems we study are not spherical and they are certainly not stationary: they are generally in a state of dynamical evolution. The possible exception to this might be the largest most isolated systems. Secondly, observed data do not have direct knowledge of the system mass except through interpreting the light that is observed. The universality of the FP allows us to turn the problem around and determine the dependence of light on mass in order that systems should fit on the FP. The simplest approach to this is to

Table 4. Scaling relation parameters and radius definition: inferred Kormendy relation parameter a and FP parameters c and d, based on the use of half-mass radius $r_{\rm half}$ and harmonic radius $r_{\rm h}$. For four different cosmologies – SCDM, ΛCDMO2, ΛCDMF2 and ΛCDMC3 – the scaling parameters and the corresponding goodness-of-fit $\mathcal{S}$ (see equations 23 and 27) are given for $r_{\rm half}$ (top row) and $r_{\rm h}$ (bottom row).

				$r \propto M^a$		$\log r_{\rm h} = c\,\mu + d\,\log\sigma_{\rm v} + C_{\rm FP}$		
Model	$\Omega_{\rm m}$	Ω_Λ	Radius	a	$\mathcal{S}_{\rm K}$	c	d	$\mathcal{S}_{\rm FP}$
SCDM	1	0	Half-mass	0.39	0.09	0.29	1.60	0.03
			Harmonic	0.38	0.06	0.37	1.78	0.03
ΛCDMO2	0.1	0.7	Half-mass	0.36	0.08	0.30	1.53	0.02
			Harmonic	0.38	0.05	0.38	1.66	0.02
ΛCDMF2	0.3	0.7	Half-mass	0.35	0.07	0.31	1.66	0.03
			Harmonic	0.36	0.05	0.41	1.88	0.02
ΛCDMC3	0.5	0.9	Half-mass	0.35	0.08	0.30	1.63	0.03
			Harmonic	0.35	0.05	0.38	1.82	0.03

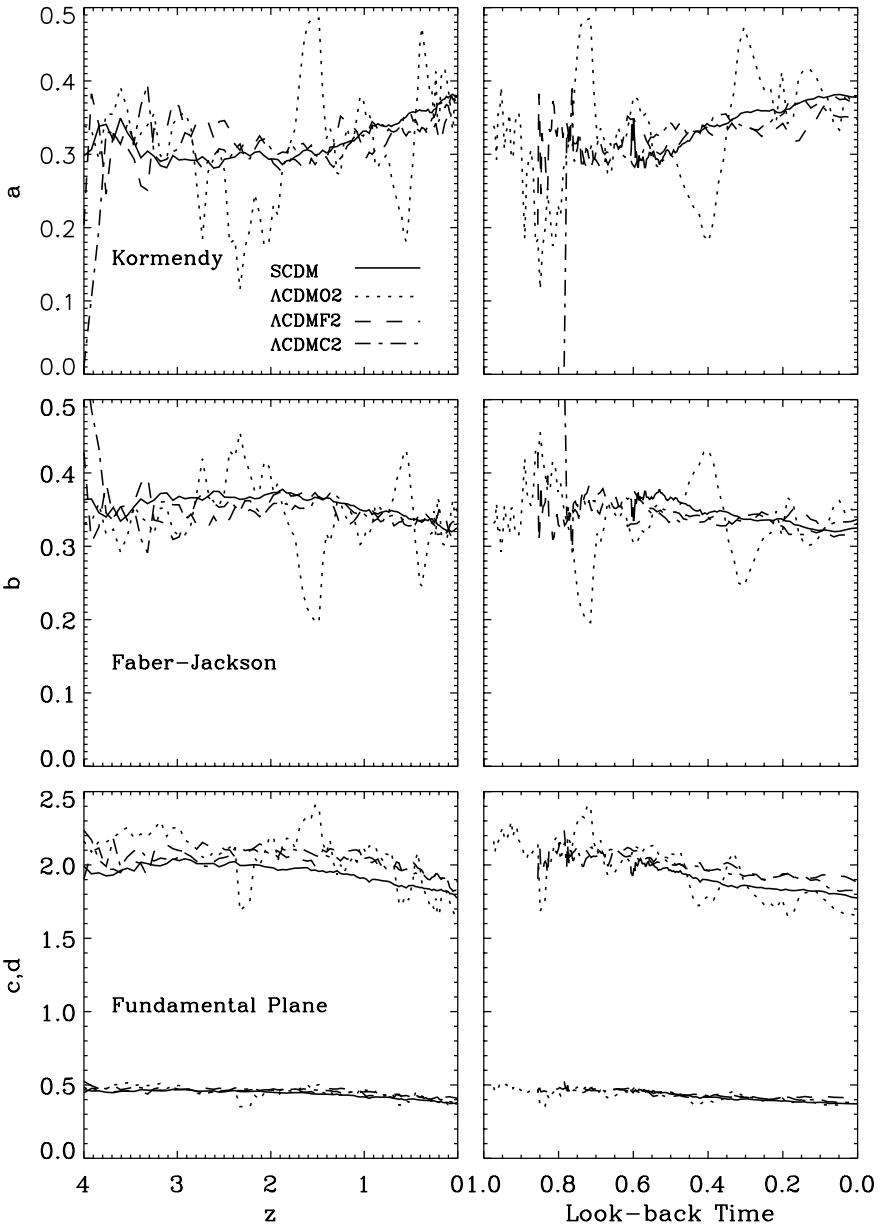

Figure 10. Evolution of the fitted scaling relation parameters as a function of redshift (left-hand column) and as a function of cosmic look-back time (right-hand column). Top panels: Kormendy parameter a. Central panels: FJ parameter b. Bottom panels: FP parameters c and d.

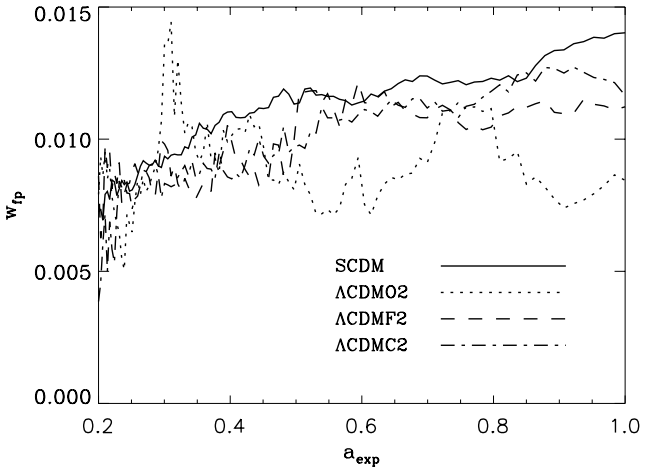

Figure 11. Evolution of the thickness of the FP for four different cosmologies. Note the almost consistently tighter FP for the low-Ω_m Universe and the modest increase of FP thickness in the other cosmologies. The SCDM, ΛCDMF2 and ΛCDMC2 models are very similar in their behaviour. The more erratic behaviour of the ΛCDMO2 may in part be due to the smaller sample size.

assume that the M/L in the observed waveband is directly related to mass.

There are further issues. For example, what do we mean when we refer to 'averages' of quantities? Using a different averaging process yields a different FP. There is also the fact that astrophysical systems are observed only in projection.

Having said that, we can express the virial theorem in terms of the variable we have used here to describe the FP. With the notation that a virialized system of mass M has a velocity dispersion V, half-mass radius $r_{\rm half}$ and harmonic radius $r_{\rm h}$, we have, up to normalizing constants,

$$V^2 = \frac{M}{r_{\rm h}^2}, \quad \Sigma = \frac{M}{r_{\rm half}^2}, \tag{32}$$

where Σ is the projected (surface) mass density. Eliminating M from these and taking logs yield an expression for the FP:

$$\log r_{\rm h} = \left(\frac{r_{\rm h}}{r_{\rm half}}\right) + 2\log V + 0.4\mu, \tag{33}$$

where we have transformed the surface mass density Σ into logarithmic astro-units via

$$\mu = -2.5\log\Sigma. \tag{34}$$

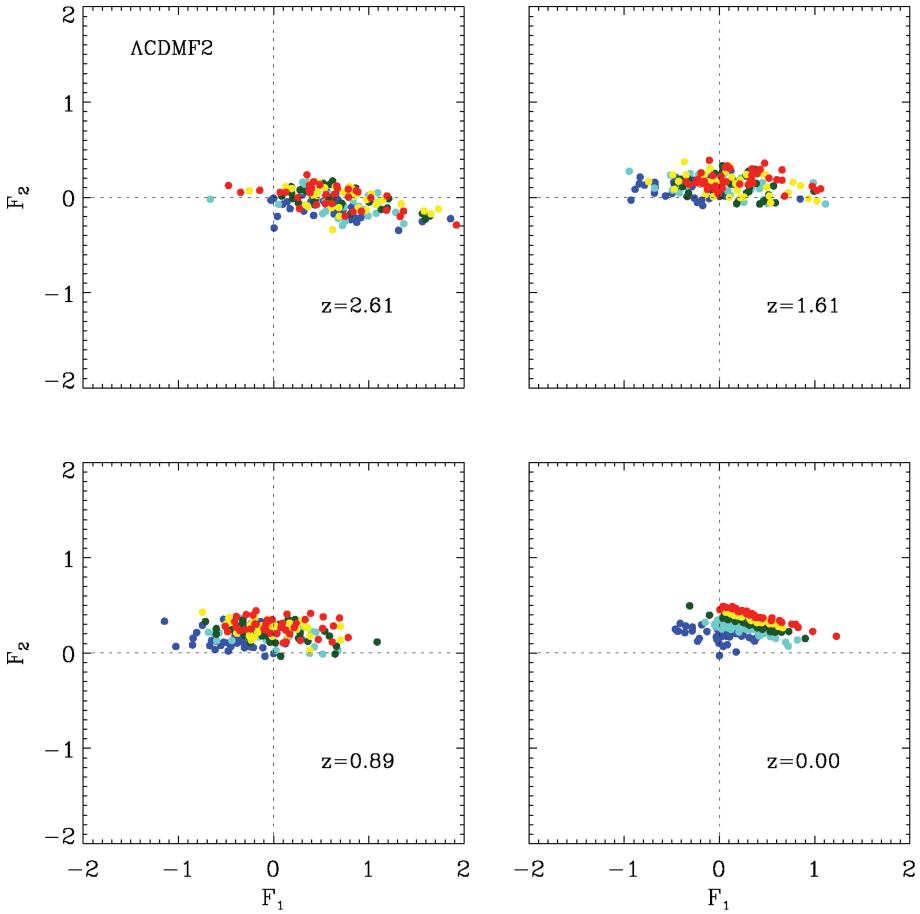

Figure 12. Shifting location of the cluster halo population within the FP. The depicted halo sample is the one in ΛCDMF2 cosmology, and is shown at four different redshifts: $z = 2.61$ (top-left panel), $z = 1.61$ (top-right panel), $z = 0.89$ (bottom-left panel) and $z = 0$ (bottom-right panel). The abscissa and ordinate axis are arbitrarily chosen, mutually perpendicular, axes within the FP plane defined by ($\log r_{\rm h}$, μ, $\log\sigma_{\rm v}$) at $z = 0$ (equation 30).

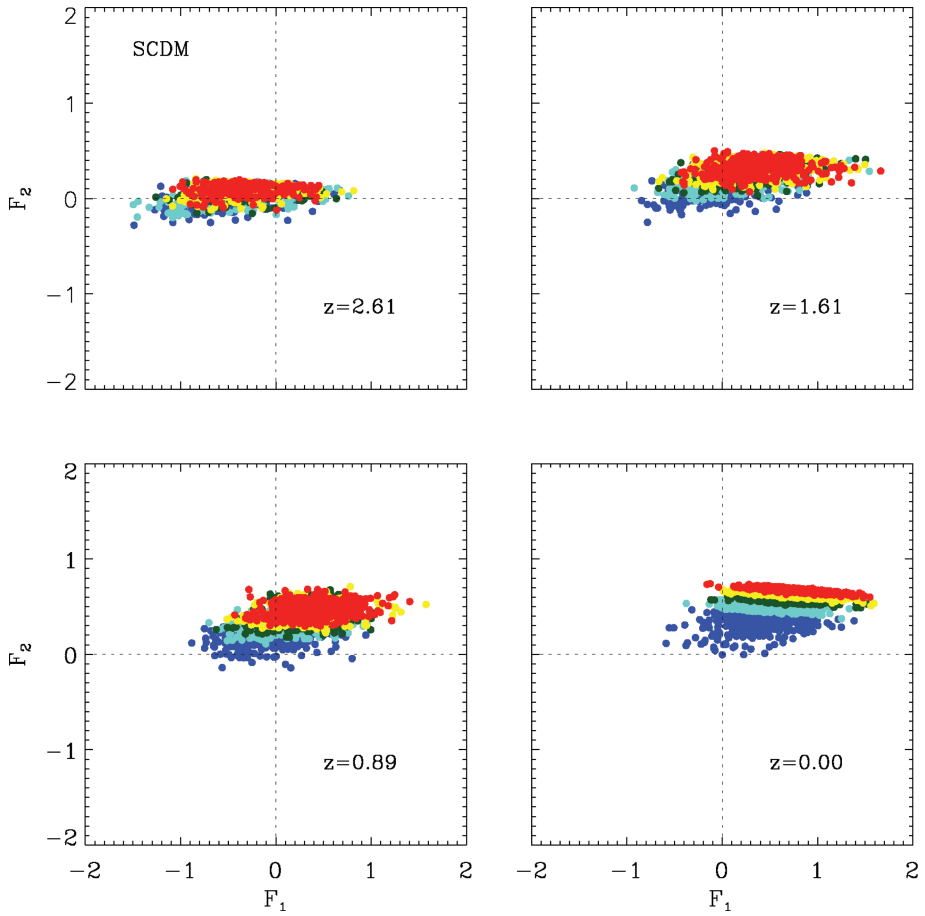

Figure 13. Shifting location of the cluster halo population within the FP. The depicted halo sample is the one in SCDM cosmology, and is shown at four different redshifts: $z = 2.61$ (top-left panel), $z = 1.61$ (top-right panel), $z = 0.89$ (bottom-left panel) and $z = 0$ (bottom-right panel). The abscissa and ordinate axis are arbitrarily chosen, mutually perpendicular, axes within the FP plane defined by ($\log r_{\rm h}$, μ, $\log \sigma_{\rm v}$) at $z = 0$ (equation 31).

We have explicitly written equation (33) in such a way as to expose the different roles of harmonic and half-mass (geometric) radii. The relationship between these radii in our models is illustrated in Figs 2 and 17, the latter differentiating between merging and quiescently accreting haloes.

7.2 Renormalizing the FP simulations

It is important to understand why the coefficients of the model FP might differ from the expectations based on the use of the virial theorem. Luminosity is not involved here, so we cannot appeal to a varying $\{M/L\}$. Moreover, the model FP is well defined, so we cannot say that this is merely a question of fitting.

There are at least two possible sources for this systematic difference between the model and the virial theorem. The first is to blame the HOP technique and assert that it systematically underestimates the cluster masses. The second is to say that the internal cluster properties (like velocity distribution) vary systematically with mass, so the normalization of the virial plane is mass-dependent.

Either way, we shall model in a mass dependency and consider this in relation to the HOP technique. The process for the variable virial normalization is analogous.

The samples of clusters derived from these simulations are all based on the HOP technique. There may well be a systematic bias in the assignment of particles to clusters (see Section 2.1). As a consequence, the radii and velocity dispersion derived for an HOP-selected cluster will also be biased. Clearly, the bias will be more significant for smaller systems.

In this section, we seek to account for systemic effects of using HOP for identifying cluster membership, and derive a renormalization procedure taking account of this and matching the data set to the expected virial theorem FP (equation 33).

The easiest way to model this bias is to assume that the model-based estimate (biased) for the mass, M, is related to the actual mass $\mathcal{M}$ by a simple scaling relationship

$$\frac{\mathcal{M}}{M} \propto \mathcal{M}^{\frac{\alpha}{1+\alpha}} \tag{35}$$

for some exponent α. The virial expression for the mass then becomes

$$V^2 = \left(\frac{\mathcal{M}}{M}\right)\frac{M}{r_{\rm h}^2} = M^{-\alpha}\frac{M}{r_{\rm h}^2}, \tag{36}$$

where the right-hand side now refers to the quantities derived from the model. We can eliminate M from this in terms of the model surface mass density $\Sigma = M/r_{\rm h}^2$ to give

$$r_{\rm h} = \left(\frac{r_{\rm h}}{r_{\rm half}}\right)^{\frac{2}{1+\alpha}} V^{2\left(\frac{1-\alpha}{1+\alpha}\right)}\,\Sigma^{-\frac{1}{1+\alpha}}. \tag{37}$$

Taking logs and using $\mu = -2.5\,\log\Sigma$ finally yield

$$\log r_{\rm h} = \frac{2}{1+\alpha}\log\frac{r_{\rm h}}{r_{\rm half}} + 2\frac{1-\alpha}{1+\alpha}\log V - \frac{0.4}{1+\alpha}\mu, \tag{38}$$

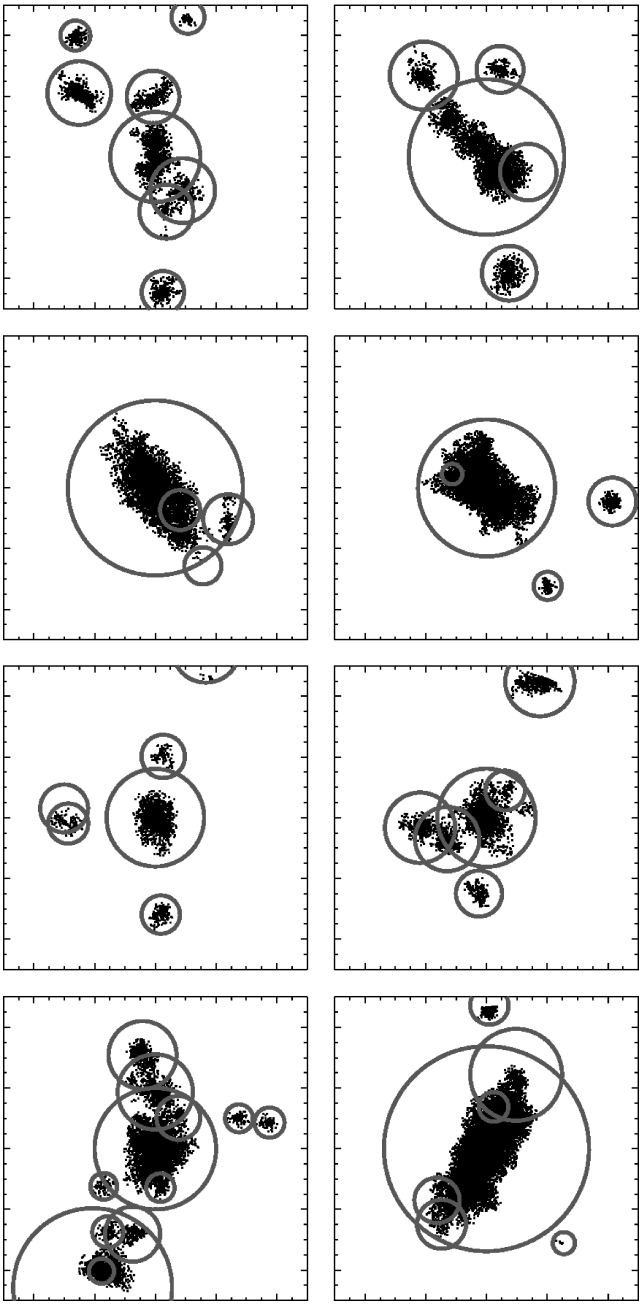

Figure 14. Accreting versus merging halo evolution: the evolution of two different haloes in the ΛCDMF2 cosmology. Each panel concerns a $5\,h^{-1}$ Mpc comoving size box centred at the core of the halo. The sequence runs from $z = 2.61$ (top-left panel), via $z = 1.61$ (top-right panel), to $z = 0.89$ (bottom-left panel) and finally the present epoch $z = 0$ (bottom-right panel). The circles indicate the location of HOP identified haloes, with the size of the circle being proportional to the (virial) radius of the halo (overlapping circles are due to the projection of the corresponding spheres). Top four panels: a quiescently evolving accreting halo. Bottom four panels: a strongly hierarchically evolving merging halo.

which is the expression for the FP in terms of the (biased) model-derived quantities. This should be compared with equation (33); we see how the bias modelled by α affects the position and slope of the virial FP.

The procedure now, for each simulation, is to select a value of α that makes the coefficient of $\log V$ in equation (38) equal to the virial value 2. That α then allows a calculation of the coefficient of μ that can be compared with the value derived from the simulation. The results for a selection of models are shown in Table 5.

The conclusion to be drawn from this is that, for each model, there is indeed a value of the α parameter that reproduces the FP fits for the models.

7.3 Observed cluster FP

The best available data set is the ENACS data of Adami et al. (1998). Equation (17) describing that FP, in the current notation, reduces to

$$\log R_{\rm e} = (0.49 \pm 0.05)\mu + (1.12 \pm 0.11)\log \sigma_{\rm v}. \tag{39}$$

There is considerable uncertainty in this relationship: the coefficient of $\log\sigma$ is quite far from the ideal 2.0 and the coefficient of μ is higher than the nominal 0.4.

The usual way to reconcile this with the virial FP is to argue that the M/L of the cluster sample is mass-dependent:

$$\frac{M}{L} \propto M^{\beta}. \tag{40}$$

Using an argument that parallels the derivation of equation (38), the FP expressed in terms of velocity and surface mass density is

$$\log r_{\rm h} = \frac{2}{1+\beta}\log\frac{r_{\rm h}}{r_{\rm half}} + 2\frac{1-\beta}{1+\beta}\log V - \frac{0.4}{1+\beta}\mu. \tag{41}$$

The data give $\beta = 0.28 \pm 0.19$ which gives rise to $c = 0.31 \pm 0.02$, a long way from the data-derived 0.49. It is clearly not possible to reconcile the ENACS data with the virial theorem FP, let alone the numerical simulations.

8 CONCLUSIONS AND DISCUSSION

We have studied three structural scaling relations of galaxy clusters in 13 cosmological models. These relations are the Kormendy relation, the FJ relation and the FP. Their validity and behaviour in the different cosmological models should provide information on the general virial status of the cluster halo population. The cosmological models that we studied involved a set of open, flat and closed Universes with a range of matter density parameter $\Omega_{\rm m}$ and cosmological constant Ω_Λ.

The cluster samples are obtained from a set of N-body simulations in each of the cosmologies. These simulations concern a box of $200\,h^{-1}$ Mpc with 256^3 dark matter particles. The initial conditions were set up such that the phases of the Fourier components of the primordial density field are the same for all simulations. In this way, we have simulations of a comparable morphological character: the same objects can be recognized in each of the different simulations (be it at a different stage of development).

After running the simulations from $z = 4$ to the current epoch using the GADGET2 code, we used HOP to identify the cluster haloes. We investigated whether each halo population obeyed a mass–radius relation akin to the Kormendy relation, a mass–velocity dispersion relation similar to the FJ relation and a two-parameter family between mass, radius and velocity dispersion that resembles an FP relation. We studied the dependence of the obtained scaling parameters as a function of the underlying cosmology and investigated their evolution in time.

Our results can be summarized as follows.

(i) In each cosmological model, we do recover Kormendy, FJ and FP relations for the population of cluster haloes. This is a strong indication that the haloes are in a virialized state, as expected in hierarchical clustering scenarios.

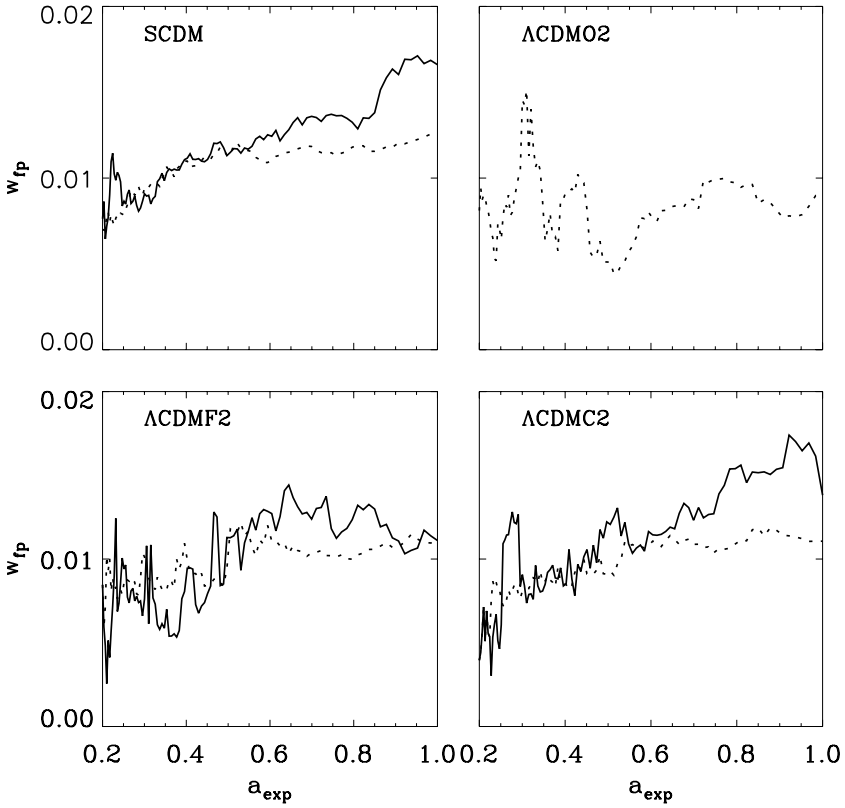

Figure 15. Thickness of the FP when considering accretion (dotted lines) or mergers (solid lines).

(ii) There are significant differences between the measured parameters of the various scaling relations and those seen in the observational data. Our fit for the FP in the ΛCMDF2 model is

$$\log r_{\rm h} = 0.41\mu + 1.86 \log \sigma + \text{constant}. \quad (42)$$

This can be reconciled with the expectation from the virial theorem, but not with the ENACS FP.

(iii) We do not find any significant dependence of the parameters a and b of the Kormendy and FJ relations on the value of $\Omega_{\rm m}$. There is also no indication for any influence of Ω_Λ on the scaling relations.

(iv) While the FP parameters c and d are not dependent on $\Omega_{\rm m}$ and Ω_Λ, there is a slight suggestion that the FP would have a lower thickness for low-$\Omega_{\rm m} \sim 0.1$ cosmologies.

(v) With the exception of low-$\Omega_{\rm m}$ Universes, we find a mild increase of the Kormendy parameter a and a mild decrease of the FJ parameter b from $z = 1$ to the present epoch. From $z = 4$ to 1, we did not find any discernable evolution.

(vi) While the FP parameters c and d, in general, do not show a significant evolution, the higher $\Omega_{\rm m}$ cosmologies do involve a slight decrease of FP parameter d during most recent epochs ($z < 2$).

(vii) The thickness of the FP does evolve significantly, with an initial increase followed by a convergence to a more ore less constant value. The convergence epoch is later for higher density cosmologies. This probably reflects the gradually virializing tendency of the cluster population.

(viii) Given our expectation that there is a difference in virial state between quiescently accreting clusters and those experiencing massive mergers, we have investigated the evolution of the FP thickness for samples of merging clusters and samples of accreting clusters. We find that accreting clusters at recent epochs do appear to be better virialized than the merging population and that the FP thickness is smaller in the former.

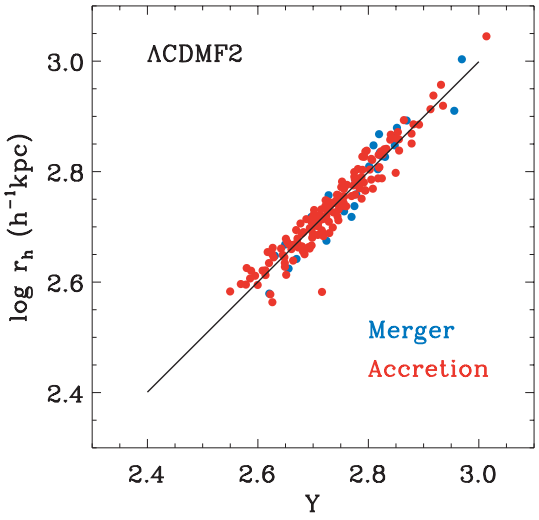

Figure 16. Comparison between the FP in the ΛCDMF2 cosmology for clusters that underwent a major merger (blue dots) and clusters that followed a more quiescent accretion history (red dots). The plot depicts the relation between harmonic radius $r_{\rm h}$ and the quantity $Y = c\mu + d \log \sigma + C_{\rm FP}$, in which c and d are the FP scaling parameters.

(ix) We find that for all investigated cosmologies the FP is remarkably stable, despite the enormous evolution of the individual systems. The only significant evolution, that of its thickness, might be due in a large part to the importance of merging of individual systems.

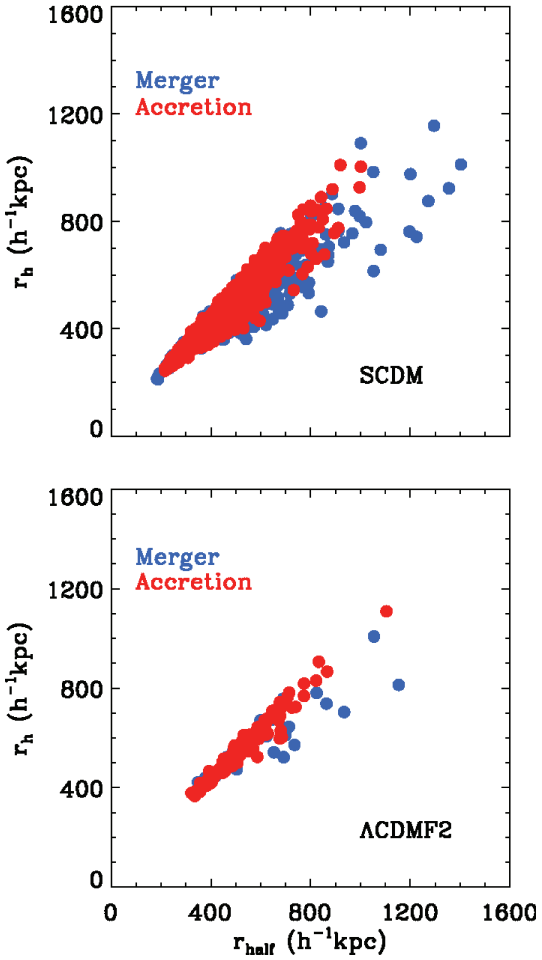

Figure 17. Comparison between the mean harmonic and the half-mass radii of the haloes in the SCDM (top panel) and ΛCDMF2 (bottom panel) scenarios. The cluster samples are split into the clusters that underwent a major merger (blue dots) and the ones that accreted matter in a more quiescent fashion (red dots) (see the text for further explanation).

Table 5. Fitting-biased models to ideal virial FP. The parameter α emulates the limitations of the HOP group finder.

Model	d	α	c	c(model)
SCDM	1.78 ± 0.01	0.058 ± 0.003	0.38	0.37 ± 0.031
ΛCMDF1	1.69 ± 0.084	0.084 ± 0.024	0.37	0.38 ± 0.016
ΛCDMF2	1.88 ± 0.04	0.031 ± 0.011	0.39	0.41 ± 0.011
ΛCDMF3	1.81 ± 0.02	0.050 ± 0.014	0.38	0.38 ± 0.056
OCDM01	1.60 ± 0.083	0.111 ± 0.024	0.36	0.35 ± 0.017

(x) If indeed the thickness of the FP might be entirely due to the merger history of the cluster haloes, the distance of an individual cluster to the FP would be a direct reflection of the cluster history.

(xi) We see direct evidence that major mergers have effected the relationship between the galaxy haloes in the cluster in that the relationship between the half-mass and harmonic radii is disturbed. None the less, the evidence from the models tells us that this does not affect the slope of the FP: clusters that have undergone major mergers lie in the same place as those that have grown by steady accretion.

Finally, what are desperately needed are better data on the cluster FP. We might speculate that the distance of a cluster from the plane defined by the data somehow reflects the evolution of the cluster, but we will not get evidence for the hypotheses derived from numerical experiment until there is more high-quality data.

ACKNOWLEDGMENTS

PAAM gratefully acknowledges support by NOVA. RvdW is grateful for the support and great hospitality of KIAS during the completion of this manuscript. In addition, BJTJ gratefully acknowledges the hospitality of the Kapteyn Astronomical Institute in Groningen, and to his collaborators for their remarkable patience in getting various parts of this paper completed.

REFERENCES

Adami C., Mazure A., Biviano A., Katgert P., Rhee G., 1998, A&A, 331, 493
Bernardi M. et al., 2003, AJ, 125, 1866
Bertin G., Ciotti L., Del Principe M., 2002, A&A, 386, 149
Binney J., Merrifield M., 1998, Galactic Astronomy/James Binney and Michael Merrifield. Princeton Univ. Press, Princeton, NJ
Bolton A. S., Burles S., Treu T., Koopmans L. V. E., Moustakas L. A., 2007, ApJ, 665, L105
Cappellari M. et al., 2006, MNRAS, 366, 1126
Djorgovski S., Davis M., 1987, ApJ, 313, 59
D'Onofrio M., 2008, ApJ, 685, 875
Dressler A., Lynden-Bell D., Burstein D., Davies R. L., Faber S. M., Terlevich R., Wegner G., 1987, ApJ, 313, 42
Eisenstein D. J., Hut P., 1998, ApJ, 498, 137
Faber S. M., Jackson R. E., 1976, ApJ, 204, 668
Faber S. M., Dressler A., Davies R. L., Burstein D., Lynden-Bell D., 1987, in Faber S., ed., Nearly Normal Galaxies: From the Planck Time to the Present, Vol. 8. Springer-Verlag, New York, p. 175
González-García A. C., van Albada T. S., 2003, MNRAS, 342, L36
Helmi A., 2000, PhD thesis, Leiden Univ.
Helmi A., White S. D. M., 1999, MNRAS, 307, 495
Jørgensen I., Franx M., Kjaergaard P., 1995, MNRAS, 276, 1341
Jørgensen I., Franx M., Kjaergaard P., 1996, MNRAS, 280, 167
Kormendy J., 1977, ApJ, 218, 333
Kormendy J., 1987, in Falber S., ed., Nearly Normal Galaxies. From the Planck Time to the Present, Vol. 8. Springer-Verlag, New York, p. 163
La Barbera F., Busarello G., Merluzzi P., Massarotti M., Capaccioli M., 2003, ApJ, 595, 127
Lahav O., Lilje P. B., Primack J. R., Rees M. J., 1991, MNRAS, 251, 128
Lanzoni B., Ciotti L., Cappi A., Tormen G., Zamorani G., 2004, ApJ, 600, 640
Marmo C. et al., 2004, in Diaferio A., ed., Proc. IAU Colloq. 195, Outskirts of Galaxy Clusters: Intense Life in the Suburbs. Cambridge Univ. Press, Cambridge, p. 242
Nigoche-Netro A., Ruelas-Mayorgo A., Franco-Balderas A., 2009, MNRAS, 392, 1060
Nipoti C., Londrillo P., Ciotti L., 2003, MNRAS, 342, 501
Perlmutter S. et al., 1999, ApJ, 517, 565
Riess A. G. et al., 1998, AJ, 116, 1009
Robertson B., Cox T. J., Hernquist L., Franx M., Hopkins P. F., Martini P., Springel V., 2006, ApJ, 641, 21
Schaeffer R., Maurogordato S., Cappi A., Bernardeau F., 1993, MNRAS, 263, L21
Spergel D. N. et al., 2003, ApJS, 148, 175
Spergel D. N. et al., 2007, ApJS, 170, 377
Springel V., 2005, MNRAS, 364, 1105
Tully R. B., Fisher J. R., 1977, A&A, 54, 661

This paper has been typeset from a TEX/LATEX file prepared by the author.